# Session 3A3
# Sensor Array Signal Processing

# Survey on Interference Mitigation via Adaptive Array Processing in GPS

**D. Lu[1,2], Q. Feng[2], and R. Wu[2]**
[1]Xidian University, China
[2]Civil Aviation University of China, China

**Abstract**—Due to the extremely low power, GPS signal can be easily affected by interferences. In this paper, from the point of adaptive array processing, we review the existing spatial and space-time interference suppression methods which attempt to mitigate interferences before the GPS receiver performs correlation. These methods comprise self-coherence restoral technique based on the nature of GPS signal, space-time minimum mean square error, power minimization technique, GPS multipath mitigation technique using the vertical array etc. Also we summarize their performance and applicability by analyzing all these techniques, in which some of our work and opinions are included.

## 1. Introduction

Global Positioning System (GPS) is a satellite-based navigation system which can provide the position, velocity and timing information for users in all weather conditions, anywhere in the world and anytime in the day. Therefore, it has been widely used in civil and military applications such as navigation by general aviation, positioning for users and so on. Because of its high precision, general acceptability and easier equipment of user's receiver, GPS will gradually become a main means of global navigation.

However, GPS signal is susceptible to interferences from either intentional or unintentional sources for the reason that it arrives at the receiver at a very low-power level, typically 20∼30 dB below the receiver's thermal noise level [1]. Based on that, the performance of GPS navigation and positioning degrades dramatically. Hence, one of the hot topic of using GPS is to cancel the interference as completely as possible without any distortion of desired GPS signal.

Conventional GPS suppression methods including time-domain and frequency-domain filtering techniques [1–4] employ DFT technology to suppress interference by taking out abnormal spectrum line of digital intermediate frequency signal. These methods have the advantages of easy implementation and low cost, but they can not mitigate multiple narrowband interferences as well as wideband interferences owing to its incapability of differentiating between desired signal and interference in the spatial domain. However, array signal processing techniques can efficiently suppress the above interferences according to the spatial information. Adaptive nulling technique [5] based on array antennas can adaptively place nulls in the direction of interferences, which is very popular to be used in improving the performance of GPS receiver. Unfortunately, the above method may be inadequate for broader band operation, especially when interference multipath is present. In order to solve this problem, space-time adaptive processing (STAP) techniques [6–9] are proposed in recent years. STAP can greatly increase the number of degrees of freedom under the equivalent antennas condition and thus can efficiently suppress wideband interference. So it is a trend of GPS interference mitigation.

This paper mainly discusses the existing methods based on adaptive array processing. The following section will describe some spatial techniques emphasis on self-coherence restoral technique using the nature of GPS signal. In Section 3 we firstly give a uniform data model, and then several STAP methods consisting of maximum signal-to-interference ratio algorithm, minimum mean square error, space-time Capon algorithm and power minimization technique are described. GPS multipath mitigation technique using the vertical array is given in Section 4. While, concluding remarks are given in Section 5.

## 2. Spatial Adaptive Processing Techniques

As demand for accurate GPS positioning, adaptive beamforming algorithm should not cause any significant distortion of the desired GPS signals when it is used to suppress interferences. Such algorithms include the direction finding algorithm [10], which is an adaptive beamforming algorithm based on estimation of the directions of arrival (DOAs) of the received signals, and directional constrained adaptive beamforming algorithm, which is based on the principle that if the dynamic of the GPS receiver is not too high and the beampattern is not too narrow, rough coordinates of the receiver and the coordinates of the satellites in view can be used to calculate the DOAs of the signals of interest from different satellites, and so on. However, these algorithms do not fully take advantage of the GPS signal structure. So Wei Sun proposed a GPS interference mitigation method using self-coherent feature of GPS signal [11, 12].

The method considers interference suppression in GPS using spatial processing that incorporates the known temporal structure of the GPS signal. And it utilizes the replication property of the C/A-code within the navigation symbol to suppress interferences which are aperiodic or have a different periodic signal structure from that of the GPS signal. A block diagram of the proposed algorithm is shown in Fig. 1, which consists of a main channel and a reference channel. The samples in the main channel and the reference channel are processed by a beamformer$\mathbf{w}$and another processor $\mathbf{f}$ respectively, where the samples of reference channel are $lP$ chips ($P = 1023,\ 1 \le l < 20$) delay of the main channel's data. These samples in the main channel are given by:

$$\mathbf{x}(n) = \mathbf{a}s(n) + \sum_{j=1}^{K} \mathbf{b}_j i_j(n) + \mathbf{v}(n) \tag{1}$$

where $\mathbf{x}(n)$ is the $M \times 1$ data vector, $s(n)$ is the desired GPS signal and $i_j(n)$ is the $j$th interference, $\mathbf{a}$ and $\mathbf{b}_j$ are $M \times 1$ steering vectors of the desired GPS signal and the jth interference respectively, and $\mathbf{v}(n)$ is the thermal noise vector. This paper provided that GPS signal, interference, and noise are uncorrelated unless special statement.

Due to the repetition of GPS signal, GPS signal samples of two channels in Fig. 1 have the same values as long as they are within the same symbol. However, the interference samples have different values because they are aperiodic or have a different periodic signal structure from that of the GPS signal. Thus the samples in the reference channel are given by:

$$\mathbf{x}(n - lP) = \mathbf{a}s(n) + \sum_{j=1}^{K} \mathbf{b}_j i_j(n - lP) + \mathbf{v}(n - lP) \tag{2}$$

The algorithm proposed can adaptively update the weight vectors $\mathbf{w}$ and $\mathbf{f}$ by maximizing the cross-correlation between the output of the main channel and the reference channel. Accordingly, we define the following cost function:

$$\mathrm{C}(\mathbf{w}, \mathbf{f}) = \frac{|R_{zd}|}{R_{zz} R_{dd}} = \frac{\left|\mathbf{w}^H \mathbf{R}_{xx}^P \mathbf{f}\right|^2}{\left|\mathbf{w}^H \mathbf{R}_{xx} \mathbf{w}\right| \left|\mathbf{f}^H \mathbf{R}_{xx} \mathbf{f}\right|} \tag{3}$$

where

$$\begin{aligned} R_{zd} &= E\left\{z(n) d^H(n)\right\} = \mathbf{w}^H E\left\{\mathbf{x}(n)\mathbf{x}^H(n - lP)\right\}\mathbf{f} = \mathbf{w}^H \mathbf{R}_{xx}^P \mathbf{f} \\ R_{zz} &= E\left\{z(n) z^H(n)\right\} = \mathbf{w}^H E\left\{\mathbf{x}(n)\mathbf{x}^H(n)\right\}\mathbf{w} = \mathbf{w}^H \mathbf{R}_{xx} \mathbf{w} \\ R_{dd} &= E\left\{d(n) d^H(n)\right\} = \mathbf{f}^H E\left\{\mathbf{x}(n - lP)\mathbf{x}^H(n - lP)\right\}\mathbf{f} = \mathbf{f}^H \mathbf{R}_{xx} \mathbf{f} \end{aligned} \tag{4}$$

The algorithm makes full use of the nature of GPS signal and does not need any knowledge of transmitted signals or the location of the satellite. Meanwhile, it is not sensitive to steering error and robust. So the algorithm is a promising method in GPS interference cancellation.

Generally speaking, spatial adaptive processing techniques are easy to implement and convenient for calculation. But it will increase array cost for an interference consuming one degree of freedom. To solve this problem, the techniques based on space-time joint processing are proposed [7–9, 13]. They all provide more degrees of freedom via time tap than only space processing.

## 3. Space-time Joint Processing Techniques

STAP algorithms employ the multiple receiving elements ("space") of an antenna array and multiple temporal samples ("time") to cancel interferences. The space-time weights are realized through a tapped-delay-line behind each antenna, as shown in Fig. 2. Some scholars, such as Dr. Fante and Dr. Zoltowski, have gained some achievements in GPS interference mitigation based on STAP [7, 8, 14]. In this section, based on the fruits of their study, we give the general space-time data model for GPS interference suppression.

### 3.1. Data Model

The space-time data model can be written as:

$$\mathbf{x}(t) = \mathbf{A}\mathbf{s}(t) + \sum_{j=1}^{K} \mathbf{B}_j \mathbf{i}_j(t) + \mathbf{V}(t) \tag{5}$$

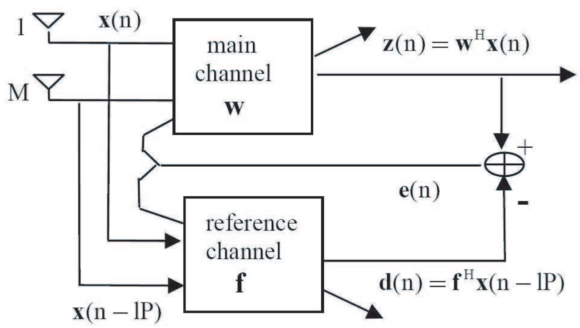


Figure 1: Block diagram of the interference suppression based on the self-coherence of GPS signal.

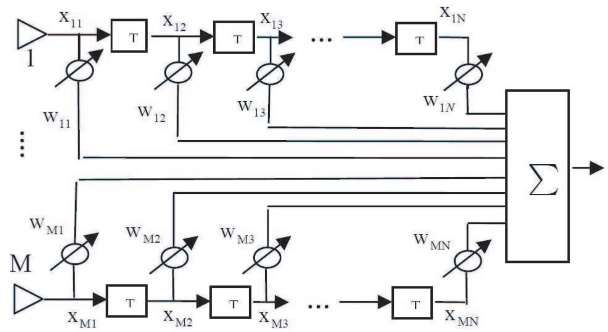


Figure 2: Block diagram of the STAP technique for GPS interference mitigation.

where $\mathbf{x}(t) = [x_{11}(t) \ldots x_{M1}(t)\, x_{12}(t) \ldots x_{M2}(t) \ldots x_{1N}(t) \ldots x_{MN}(t)]^T$ is the received data ($M$ is the number of antenna and $N$ is the number of tap each antenna), $\mathbf{A} = \mathbf{I}_{N\times N} \otimes \mathbf{a}$ and $\mathbf{s}(t) = [s(t) \ldots s(t-(N-1)T)]^T$, $\mathbf{B}_j$ and $\mathbf{i}_j(t)$ have the same structure as $\mathbf{A}$ and s$(t)$ respectively.

### 3.2. STAP Algorithm

#### 3.2.1. Maximum Signal-to-Interference-plus-Noise Ratio

This approach chooses weight vectors $\mathbf{w}$ to maximize signal-to-interference-plus-noise ratio of the output of beamformer. Accordingly, there is the following cost function:

$$\mathbf{w}_{opt} = \arg\max_{\mathbf{w}} SINR = \frac{\mathbf{w}^H\mathbf{R}_s\mathbf{w}}{\mathbf{w}^H\mathbf{R}_n\mathbf{w}} \tag{6}$$

where $\mathbf{R}_n$ is interference-plus-noise covariance matrix. Because the GPS signal strength is at least 20 dB below the thermal noise floor, $\mathbf{R}_n$ can be estimated by averaging approximately $4MN$ independent samples of the received signal [15], namely:

$$\mathbf{R}_{\rm n} \approx \mathbf{R} = E\left\{\mathbf{x}(t)\mathbf{x}^H(t)\right\} \approx \frac{1}{4MN}\sum_{q=1}^{4MN}\mathbf{x}(q)\mathbf{x}^H(q) \tag{7}$$

$\mathbf{R}_s$ is the desired GPS signal covariance matrix, which can be derived by the density of power spectrum of GPS signal. Note that this method requires information on platform attitude in order to determine $\mathbf{R}_s$, and meanwhile the processor is required being repeated for each GPS satellite which is used to determine user's position.

#### 3.2.2. Minimum Mean Square Error Algorithm

This method obtains the weight vector by minimizing the mean square error between the desired GPS signal and the output of the processor in Fig. 2. Accordingly, the cost function is given by:

$$\mathbf{w}_{opt} = \arg\min_{\mathrm{w}} E\left\{\left(s_d - \mathbf{w}^H\mathbf{x}\right)\left(s_d - \mathbf{w}^{\rm H}\mathbf{x}\right)^H\right\} \tag{8}$$

where $s_d$ is the desired signal. By solving this optimum question, we can find:

$$\mathrm{w}_{opt} = \mathrm{R}^{-1}\mathbf{g}_s \tag{9}$$

where $\mathbf{g}_s = E\left\{\mathbf{x}s_d^*\right\}$ is the first column of $\mathbf{R}_s$. Note that the processor is also repeated for each GPS satellite to calculate user's position and requires attitude information.

#### 3.2.3. Space-time Capon Beamforming

When the direction of desired GPS satellite signal can be estimated, this algorithm minimizes the output power with attempting to preserve the gain in the desired signal direction for each of the $N$ "tap times" of the processor in Fig. 2. This leads to the power minimization with $N$ linear constraints:

$$\begin{aligned}&\min_{\mathbf{w}} \mathbf{w}^H\mathbf{R}\mathbf{w}\\ &s.t.\ \mathbf{w}_i^H\mathbf{a} = 1,\ \ i = 1, \ldots, N\end{aligned} \tag{10}$$

where $\mathbf{w} = [\mathbf{w}_1, \ldots, \mathbf{w}_N]^T$, $\mathbf{w}_i = [w_{1i}, \ldots, w_{Mi}]$. And (10) can be rewritten as:

$$\begin{aligned} &\min_{w} \mathbf{w}^H \mathbf{R} \mathbf{w} \\ &s.t.\ \mathbf{w}^H \mathbf{A} = \mathbf{1}_{N\times 1} \end{aligned} \tag{11}$$

Using the method of Lagrange multipliers, the solution to (11) is:

$$\mathbf{w}_{opt} = \mathbf{R}^{-1}\mathbf{A}(\mathbf{A}^H\mathbf{R}^{-1}\mathbf{A})^{-1}\mathbf{1}_{N\times 1} \tag{12}$$

This result is similar to the one obtained by standard capon beamforming (SCB). So the approach is called space-time capon method. Like the SCB, the performance of the approach becomes worse when steering vector error exists. Therefore, some robust STAP algorithm will be developed based on the robust capon beamforming algorithm [16].

#### 3.2.4. Space-time Power Minimization Algorithm

Because the received GPS satellite signals are well below the thermal noise floor, this method is extraordinary efficient for GPS interference cancellation. It simply constraints the weight on the first tap of reference antenna 1 (see Fig. 2), and then minimizes the output power, namely:

$$\begin{aligned} &\min_{\mathbf{w}} \mathbf{w}^H \mathbf{R} \mathbf{w} \\ &s.t.\ \mathbf{w}^H \boldsymbol{\delta}_{MN} = 1 \end{aligned} \tag{13}$$

where $\boldsymbol{\delta}_{MN} = [1, 0, \ldots, 0, \ldots, 0]^T$ is the $MN \times 1$ vector. Using the method of Lagrange multipliers, the solution to (13) is

$$\mathbf{w}_{opt} = \frac{\mathbf{R}^{-1}\boldsymbol{\delta}_{MN}}{\boldsymbol{\delta}_{MN}^H \mathbf{R}^{-1}\boldsymbol{\delta}_{MN}} \tag{14}$$

This approach has the advantages of not requiring to know the DOA of the incoming GPS signal and implementing easily. So it is adopted by some available GPS antennas [13] to mitigate interference.

### 3.3. Reduced-rank STAP Technique

Because of the large dimensionality of the space-time covariance vector and weight vector, STAP techniques will lead to a larger computational burden and slower convergence. Therefore, the study on reduced-dimension techniques becomes a hot topic in recent years [8, 17]. Reduced-dimension techniques are mainly to constraint weight vector to lie in a lower dimensional subspace by the transformation matrix $\mathbf{T}_{NM\times D}$ $(D < NM)$, namely let:

$$\mathbf{w} = \mathbf{T}\mathbf{w}_r \tag{15}$$

so (13) can be rewritten as:

$$\begin{aligned} &\min_{\mathbf{w}} \mathbf{w}_r^H \mathbf{T}^H \mathbf{R} \mathbf{T} \mathbf{w}_r \\ &s.\ t.\ \mathbf{w}_r^H \mathbf{T}^H \boldsymbol{\delta}_{MN} = 1 \end{aligned} \tag{16}$$

the solution to (16) is

$$\mathbf{w}_r = \frac{(\mathbf{T}^H\mathbf{R}\mathbf{T})^{-1}\mathbf{T}^H\boldsymbol{\delta}_{MN}}{\boldsymbol{\delta}_{MN}^H\mathbf{T}(\mathbf{T}^H\mathbf{R}\mathbf{T})^{-1}\mathbf{T}^H\boldsymbol{\delta}_{MN}} \tag{17}$$

where the dimension of $\mathbf{T}^H\mathbf{R}\mathbf{T}$ is $D \times D$, which is less than the one of $\mathbf{R}$. This leads to lower computational complexity and rapid convergence. We can obtain the matrix $\mathbf{T}$ by techniques such as the cross-spectral metric (CS) or principal-components (PC). But both techniques are quite computational burden since it is necessary to generate the eigenvectors of covariance matrix before finding $\mathbf{T}$.

Fortunately, Dr. Zoltowski proposed a reduced-dimension STAP technique based on multistage nested wiener filter (MSNWF) [17]. This technique accomplishes the reduced-dimension processing via the innovative multistage wiener filter and does not require computing the inversion of $\mathbf{R}$. Thus it can reduce computational complexity and improve the speed of convergence compared with CS and PC.

## 4. GPS Signal Multipath Mitigation Techniques

The error due to GPS signal multipath is an important factor of positioning error. At the present time, the common techniques for multipath mitigation mainly include DLL and MEDLL. Both techniques change a standard receiver structure, so their compatibility is very poor. In [18] Dr. Stoica proposed a multipath mitigation algorithm based on the vertical array, which suppress multipath interference before correlation without changing the receiver structure.

The above method assumes that the directions of arrival of the GPS multipath signals are approximately known relative to the direction of arrival of the GPS signal, which is possible in GPS vertical array. When the GPS multipath signals exist, the data model received by GPS vertical array is given by:

$$\mathbf{x}(t) = \mathbf{a}s(t) + \sum_{q=1}^{Q} \mathbf{a}_q \beta_q s(t) + \sum_{j=1}^{K} \mathbf{b}_j i_j(t) + \mathbf{v}(t) \tag{18}$$

(18) can be rewritten as:

$$\mathbf{x}(t) = (\mathbf{a} + \mathbf{V}\beta)s(t) + \sum_{j=1}^{K} \mathbf{b}_j i_j(t) + \mathbf{v}(t) \tag{19}$$

where the matrix $\mathbf{V}$'s range space is a good approximation of the one spanned by the GPS multipath signals, $\beta$ is an unknown vector whose elements equal to the ratios between the GPS multipath signals and the GPS signal. According to literature [16], $\mathbf{a}$ and $\beta$ can be determined by solving the following problem:

$$\begin{aligned} &\min_{\mathbf{a},\boldsymbol{\beta}} (\mathbf{a} + \mathbf{V}\boldsymbol{\beta})^H \mathbf{R}^{-1} (\mathbf{a} + \mathbf{V}\boldsymbol{\beta}) \\ &s.\,t.\ \mathbf{a} = \mathbf{B}\mathbf{u} + \bar{\mathbf{a}}, \quad \|\mathrm{u}\|^2 \le \varepsilon \end{aligned} \tag{20}$$

let $\mathbf{G}$ be a basis of the null space of $\mathbf{V}^H$, so (20) can be rewritten as:

$$\begin{aligned} &\min_{\mathbf{a},\beta} \mathbf{a}^H \mathbf{G} \left(\mathbf{G}^H \mathbf{R} \mathbf{G}\right)^{-1} \mathbf{R}^{-1} \\ &s.\,t.\ \mathbf{a} = \mathbf{B}\mathbf{u} + \bar{\mathbf{a}}, \quad \|\mathrm{u}\|^2 \le \varepsilon \end{aligned} \tag{21}$$

let $\hat{\mathbf{a}}$ denotes the solution to (21), we can find the weight vector:

$$\mathbf{w} = \mathbf{G}(\mathbf{G}^H \mathbf{R} \mathbf{G})^{-1} \hat{\mathbf{a}} \tag{22}$$

In essence, the method proposed by Dr. Stoica removes the GPS multipath signals by "pre-filtering" the received data via the matrix $\mathbf{G}^H$. Although this algorithm is appropriate to GPS vertical array, its main idea can be further extended to the general array to suppress GPS multipath signals.

## 5. Conclusion

Several methods used to mitigation GPS interference have been discussed in this paper. The conventional spatial techniques can adaptively null the interference, but they are incapability of canceling many narrowband interferences as well as wideband and mutipath ones due to the limited degrees of freedom. STAP can overcome the above problem. However, the computational complexity is a troublesome question. Fortunately, the reduced-dimension technique proposed by Dr. Zoltowski has made a breakthrough in GPS interference mitigation. Different from the above reduced-dimension method, the next work we will do is to develop an adaptive recursive least square (RLS) space-time algorithm combined with cyclostationary properties of GPS signal, which will improve speed of convergence by RLS algorithm. Also the algorithm belongs to blind adaptive algorithm by only using the nature of GPS signal, so it is very robust.

## Acknowledgment

This work was supported in part by the National Natural Science Foundation of China under grant 60325102 and 60428101.

### REFERENCES

1. Capozza, PT, BJ Holland, TM Hopkinson and etc., "A single-chip narrow-band frequency-domain excisor for a global positioning system (GPS) receiver," *IEEE Journal of Solid-state Circuits*, Vol. 35, No. 3, 2000.
2. Milstein, L. B., "Interference rejection techniques in spread spectrum communications," *Proc. IEEE*, Vol. 76, No. 6, June 1988.

3. Crochiere, R. E. and L. R. Rabiner, "Multirate digital signal processing," Prentice-Hall, Inc., Englewood Cliffs, New Jersey, 1983.
4. Jones, W. W., and K. R. Jones, "Narrowband interference suppression using filter-bank analysis/synthesis techniques," *IEEE MILCOM Conference*, San Diego, California, Paper 38. 1. 1, 1992.
5. Brown, A., D. Reynolds, et al., "Jammer and interference location system-design and initial test result," *Proceeding of the ION GPS'99[C]*, Nashville, TN, 1999.
6. Fante, R. L. and J. J. Vaccaro, "Cancellation of jammers and jammer multipath in a GPS receiver," *IEEE AES System Magazine*, Vol. 13, 25–28, November 1998.
7. Fante, R. L. and J. J. Vaccaro, "Wideband cancellation of interference in a GPS receiver array," *IEEE Transaction on Aerospace and Electronic Systems*, Vol. 36, No. 2, 549–564, April 2000.
8. Myrick, W., J. Goldstein, and M. Zoltowski, "Low complexity anti-jam space-time processing for GPS," *Proceedings of the 2001 IEEE International Conference on Acoustics, Speech, and Signal Processing*, Vol. 4, 1332–1336, 2001.
9. Moelker, D., T. van Der Pol, and Y. Bar-Ness, "Adaptive antenna arrays for interference cancellation in GPS and GLONASS receivers," *Proceeding of the IEEE 1996 Position Location and Navigation Symposium*, 191–198, 1996.
10. Wang, Y., JR Cruz, "Adaptive antenna array for cellular CDMA communication system," *Proc. IEEE ICASSP*, 1725–1728, July 1995.
11. Sun, W. and M. Amin, "GPS interference suppression using self-coherent feature of GPS signals," *IEEE International Symposium on Signal Processing and Information Technology*, Darmstadt, Germany, Dec. 2003.
12. Sun, W. and M. Amin, "A self-coherence based anti-jam GPS receiver," *IEEE Transactions on Signal Processing*, 62–65, 2003.
13. Hatke, G., "Adaptive array processing for wideband nulling in GPS system," *Proceedings of the 32nd Asilomar Conference on Signals, Systems and Computers*, Vol. 2, 1332–1336, 1998.
14. Myrick, W., M. D. Zoltowski, and J. S. Goldstein, "Smoothing of space-time power minimization based preprocessor for GPS," *Second Joint USA/Australia Workshop in Defense Application of Signal Processing (DASP99)*, Chicago, IL, Starved Rock State Park, 125–130, 22–26, August 1999.
15. Brenna, L., J. Mallett, and L. Reed, "Adaptive arrays in airborne MTI radar," *IEEE Transactions on Antennas and Propagation*, 607–615, April 1976.
16. Li, J., P. Stoica, and Z. Wang, "On robust capon beamforming and diagonal loading," *IEEE Transactions on Signal Processing*, Vol. 51, 1702–1715, July 2003.
17. Myrick, W., M. D. Zoltowski and J. S. Goldstein, "Anti-jam space-time preprocessor for GPS based on multistage nested wiener filter," *Milcom'99*.
18. Jiang, Y. and P. Stoica, "Capon beamforming in the presence of steering vector errors and coherent signals," http://www.sal.ufl.edu/yjiang/papers/R2CBASAP.pdf.

# A Simulation Tool for Space-time Adaptive Processing in GPS

**W. Y. Zhao**, **L. F. Xu**, **and R. B. Wu**
Civil Aviation University of China, China

**Abstract**—With the wide use of GPS, it becomes more and more important to improve the positioning accuracy. The GPS signal is very weak, and can be easily interfered. Space-time adaptive processing(STAP) can suppress the jamming not only in the temporal domain, but also in the spatial domain. STAP has now become a good candidates for jamming mitigation in GPS.

In order to evaluate the performance of various kinds of STAP algorithms, and to develop the novel STAP algorithms. we need to simulate space-time array GPS data with high fidelity and the software GPS receiver. This paper mainly presents a simulation method for space-time GPS data, as well as the simulation of some typical kinds of jammers. The simulation method for software GPS receiver is also introduced. The data that after the process of STAP is computed by the simulated GPS receiver. The simulation results show that the simulation tool is a good platform for the development of STAP algorithms.

## 1. Introduction

GPS is a network which is composed of many satellites, it can provide accurate position and time information [1]. The signal received by GPS receiver has the characteristics not only in temporal domain, but also in spatial domain. With the advent of STAP algorithms, the jammings can be suppressed through spatial and temporal characteristics effectively, and the positioning precision can be further improved. To evaluate the effect of the STAP algorithms on GPS jamming mitigation, we set up this simulation platform for Space-Time array GPS data. Besides we also simulate the software GPS receiver to validate the data after being processed by algorithms [2, 3].

In the second section of this paper, the simulation method for Space-Time array data is introduced. In the third section we introduce the common jammings to the GPS and simulate some typical of them. In the forth section we introduce the simulation method of GPS receiver briefly. The simulation results are given in the fifth section and in the sixth section we get the conclusion.

## 2. The Method for Simulating Space-time Array Data

### 2.1. Single Channel Temporal GPS Data Generation

The GPS signal is composed of navigation data, PRN code and carrier for modulation. The navigation data is a binary coded file, and is transmitted in frames according to certain format. It contains ephemeris parameters, satellite almanac and so on. We can compute the satellites position with them. These parameters value can be found from related data resources. In this paper, we choose the data from CDDIS (http://cddisa.gsfc.nasa.gov). They are coded in RINEX format. We should find the corresponding parameters from them first. These parameters, multiply by themselves scale factors, are converted to binary bits that fit the navigation data format. We only need to simulate the first three sub-frames [3].

The GPS signal is of two kinds of PRN codes, that is C/A code and P code. The structure of P code is quite complex and secret to civil users. Here we only introduce the simulation of C/A (coarse/acquisition) code. The C/A code is coded in binary format, and has the characteristics of multi address, searching GPS signal, coarse acquisition and anti-jamming. It is generated by two 10-order feedback shift registers, which can generate $C_{10}^2 + 10 = 55$ kinds of different C/A code [3]. The 24 satellites have different C/A codes. The chip shift between the satellites is fixed. According to one satellite's C/A code, we can obtain the others' C/A codes.

After the navigation data is spread by the C/A code, they modulate the carrier centered at 1575.42 MHz by BPSK. Since the data we need is at the intermediate frequency that after down-conversion, we select it as $f_{IF} = 21.25$ MHz. And after band-pass sampling, the output center frequency is $f_0 = 1.25$ MHz. The power of the signal arrived at the receiver is about -155 db. We select the gain of the receiver antenna as 4 db, and the gain of its' amplifier as 31 db. Thus the signal at IF is -120 db. Once assume the position of the receiver, we can get the propagation time of the GPS signal.

### 2.2. Multiple Channel Space-time GPS Data Generation

Suppose the signal of a GPS Satellite arrive at the receiver antenna with the direction of $\theta$, the expression of it is $f(t)$, refer to Fig. 1. So the signal that reaches the second antenna [4] is $f(t-\tau)$, $\tau = l/c$, $l = d\cos(\theta)$, where $\tau$ denotes the arrival time difference between the first antenna and the second antenna, and $d$ denotes the inter-element distance. So the signal received by the second antenna can be expressed as $f(t - d\cos(\theta)/c)$, approximately to $f(t)e^{-j\omega\tau} = f(t)e^{-j2\pi f \times d\cos(\theta)/c}$.

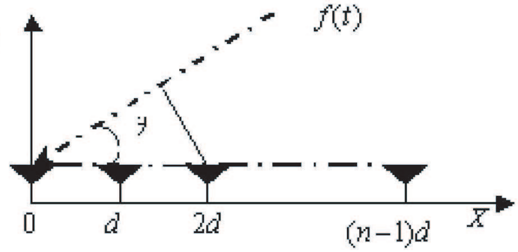

Figure 1: Uniform linear array.

Similarly, the signal of the satellite that arrives at the $n$th antenna can be expressed as:

$$f(t)e^{-j\omega(n-1)\tau} = f(t)e^{-j2\pi f\times(n-1)d\cos(\theta)/c} \tag{1}$$

Suppose that every antenna has M time delays, and each time delay is $T$, so the Space-Time satellite data can be expressed as:

$$F(t,\theta) = \begin{pmatrix} f(t) \\ f(t-T) \\ \cdots \\ f(t-(M-1)T) \end{pmatrix} \begin{pmatrix} 1 & e^{-j\omega\tau} & \cdots & e^{-j\omega(N-1)\tau} \end{pmatrix} \tag{2}$$

As for the arrived signal that contains four GPS satellites, its' multiple channel Space-Time data model can be expressed as:

$$S(t,\theta) = \sum_{i=1}^{4} \begin{pmatrix} f_i(t) \\ f_i(t-T) \\ \cdots \\ f_i(t-(M-1)T) \end{pmatrix} \begin{pmatrix} 1 & e^{-j\omega\tau_i} & \cdots & e^{-j\omega(N-1)\tau_i} \end{pmatrix} \tag{3}$$

where $f_i(t)$ denotes the $i$th satellite signal received, $\tau_i$ denotes the $i$th of the satellite time delay.

## 3. Jamming Simulation

During the GPS signal propagation, it can be affected by Satellite Clock error, Ionospheric error, multi-path jamming, radio station RF jamming, noise and so on. The typical jamming sources are broadcast TV–UHF channel, air-borne VHF, personnel electronic device, Ultra broadband communication, Multi-path, etc. For the purpose of build Space-Time data platform, we only consider narrowband RF jamming, broadband FM jamming, and receiver random noise.

Take the broadband FM jamming for example, its' model can be expressed as:

$$J(t) = A_0 \cos[\omega_0 t + k_f \int_0^t V_\Omega(t)dt] \tag{4}$$

The system frequency scope is $\omega_0 - k_f \mid V_\Omega \mid \leq \omega \leq \omega_0 + k_f \mid V_\Omega \mid$. On the basis of typical value, the jamming requires lowest power lever and has the worst affection when the frequency bias is between 400 K–600 K. So we select the biased frequency $\Delta f = 500\,\text{MHz}$, centered frequency $f_0 = 1.2\,\text{MHz}$, and the jamming power is 60 db above the signal power, that is -60 db.

As the single channel temporal data extend to multiple channel Space-Time data, we also need to extend the jamming into multiple channel Space-Time form, its' mathematical model can be expressed as:

$$I(t,\theta) = \sum_{i=1}^{m} \begin{pmatrix} J_i(t) \\ J_i(t-T) \\ \vdots \\ J_i(t-(M-1)) \end{pmatrix} A_i(\theta) \tag{5}$$

where $A_i(\theta)$ denotes the steering vector of the jamming.

The receiver internal noise $n(t)$ obeys Gauss statistical distribution, it can occupy the whole frequency. The Space-Time GPS data with jamming can be expressed as:

$$D(t,\theta) = S(t,\theta) + I(t,\theta) + n(t) \tag{6}$$

## 4. The Simulation Method of Software GPS Receiver

In the simulation of software GPS receiver, we take the advantage of the flexibility of software. We mainly introduce the acquisition and tracking modules.

The traditional acquisition is a two-dimensional search process. The computation amount is quite large. Based on the software, we use the circular correlation method, showed as Fig. 2.

Assume the input signal is $y_k$. We take the local carrier at $f_i$ as $l_{i,k} = exp(j2\pi f_i t_k)$. First the FFT result of $N$ points of $y_k \cdot l_{i,k}$ is multiplied by the conjugate FFT of the $N$ points of local C/A code. Then the IFFT of the product gives the correlation result in the time domain for all the 1023 code phase offsets.

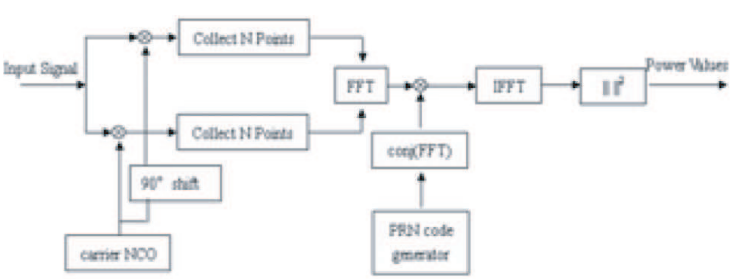


Figure 2: Acquisition based on circular correlation.

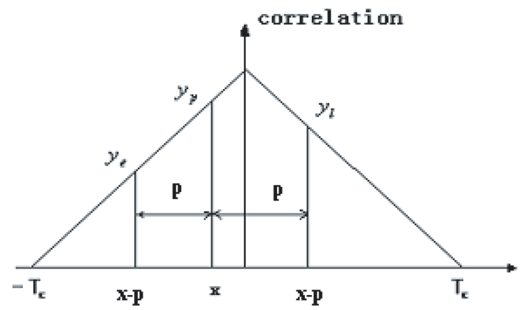


Figure 3: The correlation curve.

In the code tracking module [5], we use the numerical relation of correlation values of prompt code, early code and late code with the input IF sampled signal to adjust the input signal and get the finer code phase offsets $x$ instead of traditional DLL. Assume the correlation values are $y_p$, $y_e$, $y_l$ respectively. The relationship of them is showed as Fig. 3, where $T_c$ is the code chip width, $p$ is the code offset between prompt code and early/late code. From Fig. 3, we obtain that

$$r = \frac{y_l}{y_e} = \frac{T_c - x - p}{T_c + x - p} \Rightarrow x = \frac{(1-r)(T_c - p)}{1-r} \tag{7}$$

From $x$, we shift the input signal left or right one sample, and can evaluate the finer code phase error.

Due to the flexibility of software, we use third-order PLL to fit the high dynamic situation. We choose the loop filter as $F(s) = \frac{1+s\tau_2}{s\tau_1} \cdot \frac{1+s\tau_4}{s\tau_3}$, So the error transfer function is $H_e(s) = \frac{\tau_1\tau_3 s^3}{\tau_1\tau_3 s^3 + K\tau_2\tau_4 s^2 + K(\tau_2+\tau_4)s + K}$, where $K$ is the loop gain. Let $a = \frac{K}{\tau_1\tau_3} = \omega_n^2\eta$, $b = a(\tau_2+\tau_4) = \omega_n^2 + 2\zeta\omega_n\eta$, $c = a \cdot \tau_2\tau_4 = 2\zeta\omega_n + \eta$, and we can get

$$H_e(s) = \frac{s^3}{s^3 + cs^2 + bs + a} = \frac{s^3}{(s+\eta)(s^2 + 2\zeta\omega_n s + \omega_n^2)} \tag{8}$$

From the formula (8), we can choose the $\zeta$, $\omega_n$ and $\eta$ according to the dynamic situation easily.

## 5. Simulation Results

In this paper, we choose the digital centered frequency as 1.25 MHz. According to Shannon sampling theorem, we choose acquisition frequency as 5 MHz, the power of jamming 60 db above that of GPS signal, that is -60 db. The receiver internal noise 20 db above that of GPS signal, that is -100 db. The Fig. 4 denotes the waveform of GPS data without jamming on one antenna. And the Fig. 5 denotes the waveform of GPS data with Broadband FM jamming on one antenna. Their spectrums that are with and without the broadband jamming are indicated in Fig. 6 and Fig. 7 respectively. In the experiment, we choose the antenna position as (X:-3173088.339 m;Y:-3625066.392 m;Z:4181362.566 m), and the position computed by our software receiver is(X:-3173092.972m; Y:-3625044.536 m; Z: 4181358.520 m). The Fig. 8 denotes the spectrum of GPS data after STAP processing.

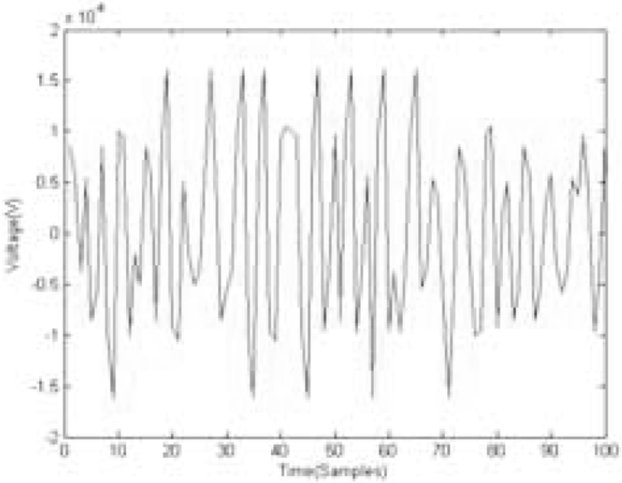


Figure 4: Waveform of Space-Time GPS data without jamming.

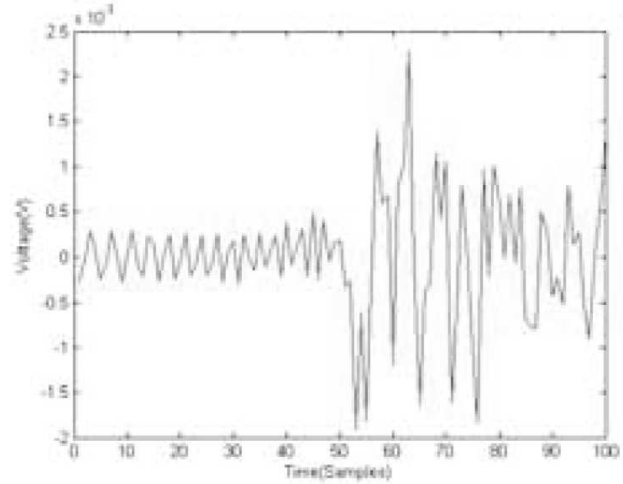


Figure 5: Waveform of Space-Time GPS data with broadband FM jamming.

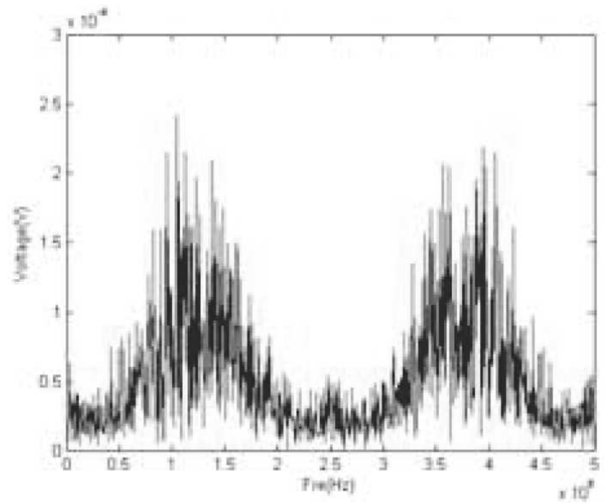


Figure 6: Spectrum of Space-Time GPS data without jamming.

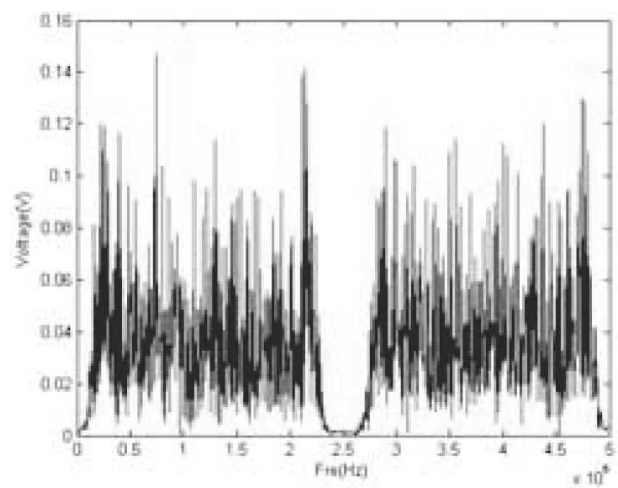


Figure 7: Spectrum of Space-Time GPS data with broadband FM jamming.

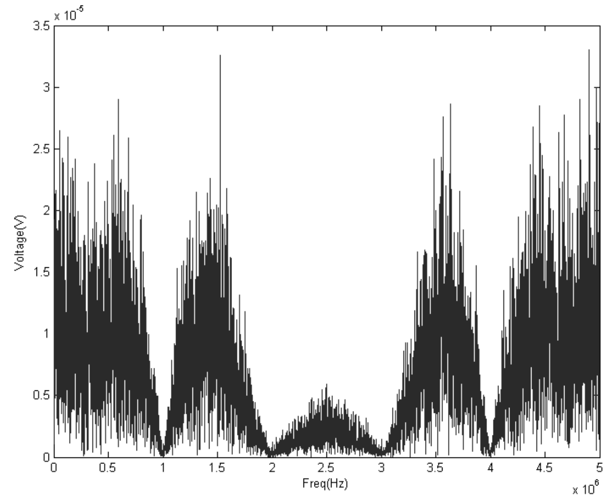


Figure 8: The spectrum of GPS data after STAP processing.

## 6. Conclusion

The simulation result shows that the Space-Time array data simulation method is valid and of high fidelity. And the simulation tool has been testified as a good platform for evaluating the STAP algorithms and using them in GPS. It will be of great help to improve the GPS positioning precision further.

## Acknowledgement

This work was supported in part by the National Science Foundation of China under grant 60325102 and 60428101.

### REFERENCES

1. Kim, S.-J. and R. A. Iltis, "Space-Time adaptive processing for GPS receiver synchronization and interference," University of California Doctoral thesis, California, 2002.
2. Hake, G. F., and A. F. Yegulalp, "A novel technique for simulating Space-Time array data," *IEEE Transaction on Communications*, 542:546, 2000.
3. Dong, L., "IF GPS signal simulator development and verification," UCGE Reports, Number 20184, 2003.
4. Krim, H. and M. Viberg, "Two decades of array signal processing research," *IEEE on SP*, 67:95, July 1996.
5. Tsui, J. B.-Y., "Fundamentals of global positioning system receivers: a software approach," A Wiley Interscience Publication, New York, 2000.

# Analysis and a Novel Design of the Beamspace Broadband Adaptive Array

**W. Liu**[1], **R. B. Wu**[2], **and R. Langley**[1]
[1]University of Sheffield, UK
[2]Civil Aviation University of China, China

**Abstract**—An analysis of the broadband beamspace adaptive array is provided. There are two conditions imposed on the array. First, the individual beams should have a good frequency invariant property. Second, they should be linearly independent. However, these two conditions are not independent and it is shown that there is a trade-off between them. To improve the interference cancellation capability of the array, we may need to sacrifice the frequency invariant property of the beams to some degree for more linearly independent beams. A DFT-modulated design method is also proposed, where the beam directions are uniformly distributed over the spatial domain and the linear independence of the beams is guaranteed inherently. Simulation results verified our analysis and the proposed method.

## 1. Introduction

Adaptive beamforming has found numerous applications in various areas ranging from sonar and radar to wireless communications [1]. For arrays to accomplish nulling over a wide bandwidth, tapped-delay lines (TDLs) are employed, resulting in an array with $M$ sensors and TDLs of length $J$, as shown in Fig. 1. To perform beamforming with high interference rejection and resolution, we need to employ a large number of sensors and long TDLs, which unavoidably increases the computational complexity of its adaptive part and slows down the convergence of the system. To reduce the computational complexity of a broadband adaptive beamformer and increase its convergence speed, Many methods have been proposed, including the time-domain subband adaptive beamformer [2, 3], a combination of subband decomposition in both the temporal and spatial domains [4], and those based on frequency invariant beamforming techniques [5, 6].

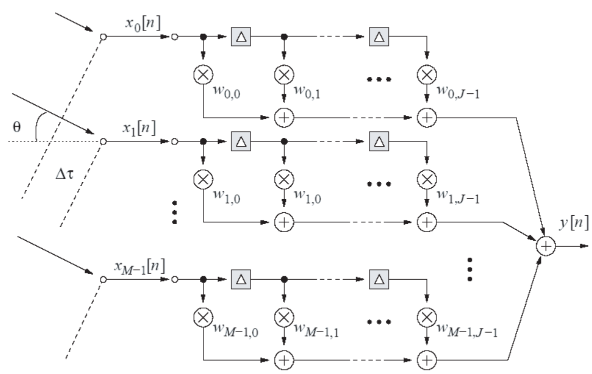


Figure 1: A signal impinges from an angle $\theta$ onto a uniformly spaced broadband linear array with $M$ sensors, each followed by a $J$-tap filter.

As the broadband counterpart of the narrowband beamspace adaptive array, the beamspace broadband adaptive array was proposed in [5], where several frequency invariant beams (FIBs) are formed pointing to different directions by a fixed beamforming network with two-dimensional (2-D) filters; thereafter the outputs of these beams are combined adaptively by a single weight for each of them. Since both the number of beams and the number of selected beams are small, the total number of adaptive weights is greatly reduced.

In this paper, we will first give an analysis of the broadband beamspace adaptive array to show a trade-off between two conditions imposed explicitly or implicitly and its impact on the performance of the resultant beamformer. It can be proved that the number of independent beams formed is the same as the length $N$ of the prototype filter for the fan filter design. Although we can design as many frequency invariant beams as we want, only $N$ of them are independent and at most we can only null out $N-1$ interfering signals. As the array's interference cancellation ability is dependent on both the number of independent beams and the frequency invariant property of those beams, we can sacrifice the frequency invariant property to some degree to design more independent beams. As a result, the array's interference cancellation property will be improved. With the above analysis, we then propose a new design of the frequency invariant beams, where their beam directions are uniformly distributed in the spatial domain and their independence is guaranteed inherently by the special form of the prototype filters, which are derived from another prototype filter by the discrete Fourier transform (DFT) modulation with appropriately imposed zeros.

This paper is organised as follows. A brief review of the broadband beamspace adaptive array is provided in Section. An analysis of the trade-off in its design is given in. The design based on the DFT modulation is proposed in Section. Design examples and simulation results are given in Section, and conclusions drawn in Section.

## 2. Broadband Beamspace Adaptive Array

In a narrowband beamspace adaptive array [7], a total of $N$ beams are formed by a beamforming network, where one is the main beam pointing to the direction of the signal of interest and the remaining $N-1$ beams are auxiliary beams pointing to the remaining directions. The output power levels of the auxiliary beams are compared to a threshold and those higher than the threshold will be chosen in the following adaptation. In this way the resultant partially adaptive array can maintain an acceptable performance with a lower computational complexity. Extend this idea to the broadband case, we can also design $N$ broadband beams pointing to different directions to form a broadband beamspace adaptive array. To combine the outputs of the beams with one adaptive weight for each of them, their response should be frequency invariant.

In [5], such a broadband beamspace adaptive array was proposed for an equally spaced linear array. With the recent development in the design of frequency invariant beamformers for one-dimensional (1-D), two-dimensional (2-D) and three-dimensional (3-D) arrays [8], we can easily extend the idea of a beamspace adaptive array to the 2-D and 3-D cases. Here we will focus on the case of a linear array and first we give a brief review of the proposed beamspace approach.

Suppose a signal with an angular frequency $\omega$ and an angle of arrival $\theta$ impinges on the uniformly spaced linear array of Fig. 1, then its output in continuous form can be written as

$$y(t) = e^{j\omega t} \sum_{m=0}^{M-1} \sum_{k=0}^{J-1} w_{m,k} \cdot e^{-jm\omega\Delta\tau} \cdot e^{-jk\omega T_s} \tag{1}$$

with $\Delta\tau = \dfrac{d}{c}\sin\theta$, where $T_s$ is the delay between adjacent samples in the TDL, $d$ is the array spacing, and $c$ is the wave propagation speed. Then the array's response can be written as

$$\tilde{R}(\omega,\theta) = \sum_{m=0}^{M-1} \sum_{k=0}^{J-1} w_{m,k} \cdot e^{-jm\omega\Delta\tau} \cdot e^{-jk\omega T_s}. \tag{2}$$

With the normalised angular frequency $\Omega = \omega T_s$, we obtain the response as a function of $\Omega$ and $\theta$

$$R(\Omega,\theta) = \sum_{m=0}^{M-1} \sum_{k=0}^{J-1} w_{m,k} \cdot e^{-jm\mu\Omega\sin\theta} \cdot e^{-jk\Omega} \quad \text{with} \quad \mu = \frac{d}{cT_s}. \tag{3}$$

With the substitution of $\Omega_1 = \Omega$ and $\Omega_2 = \mu\Omega\sin\theta$ in (3), we obtain a 2-D digital filter response

$$R(\Omega_1,\Omega_2) = \sum_{m=0}^{M-1} \sum_{k=0}^{J-1} w_{m,k} \cdot e^{-jk\Omega_1} \cdot e^{-jm\Omega_2}. \tag{4}$$

We see that the spatio-temporal spectrum of the received signal lies on the line $\Omega_2 = \mu\Omega_1\sin\theta$. Suppose the desired frequency invariant response of the array is $P(\sin\theta)$. By the substitution $\sin\theta = \left(\frac{\Omega_2}{\mu\Omega_1}\right)$, we can obtain the response $R(\Omega_1,\Omega_2)$ with nominal parameters $\Omega_1$ and $\Omega_2$. Sample the function $R(\Omega_1,\Omega_2)$ at the $(\Omega_1,\Omega_2)$ plane and then apply an inverse discrete Fourier transform (DFT) to the resultant 2-D data, we will then find the corresponding coefficients $w_{m,k}$. To fit the spatial and temporal dimensions of the array, we may need to truncate the result from the inverse DFT [5, 8].

For the desired response $P(\sin\theta)$, it can comes from a 1-D digital filter $H(e^{j\Omega})$ by the substitution $\Omega = \pi\sin\theta$. If $H(e^{j\Omega})$ is a lowpass filter [5], then signals from the directions around $\theta = 0$ will correspond to its passband, and a beam is formed pointing to the direction $\theta = 0$. If we want to steer this beam to the direction $\theta = \theta_0$ with the same low pass filter $H(e^{j\Omega})$, we can vary it into the form $\tilde{H}(e^{j\pi\sin\theta}) = H(e^{j(\Omega-\pi\sin\theta_0)})$ and consider $\tilde{H}(e^{j\pi\sin\theta})$ as the new desired frequency invariant response.

As the sampling frequency is in general twice the highest frequency component of the signal and array spacing is half the wavelength of the highest frequency component, we have $d = \frac{1}{2}\cdot c\cdot(2T_s) = cT_s$ and $\mu = 1$. Therefore, without loss of generality, we will only consider the case with $\mu = 1$ in the design and simulations.

Moreover, we also assume the signal of interest comes from the broadside, then the main beam will point to the direction of $\theta = 0$. For the auxiliary beams, their directions are decided in such a way that the main direction of a beam should ideally coincide with nulls (zero responses) of all other beams, as mentioned in the simulation part of [5].

A single adaptive weight is applied to each of the auxiliary beams by minimizing the variance of the error signal between the main beam and the auxiliary beams. In the adaptation, some of the auxiliary beam outputs are active and some others are simply discarded if their output signals are below some prescribed level. Fig. 2 shows the diagram of such a broadband beamspace adaptive array, where $\mathbf{x}[n]$ is the vector containing the received signals $x_0[n], \ldots, x_{M-1}[n]$ and $w_1, \ldots, w_{P-1}$ are the adaptive weights attached to each of the beam outputs.

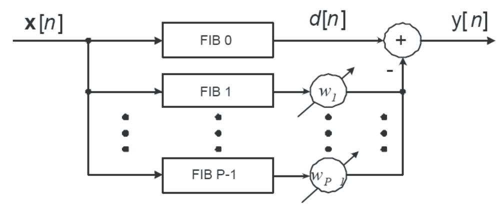


Figure 2: A broadband beamspace adaptive array with $P$ frequency invariant beams (FIBs).

## 3. Analysis of the Broadband Beamspace Adaptive Array

For the beamspace array to work, the frequency invariant beamforming network needs to meet two conditions, which are imposed explicitly or implicitly.

First, the beams formed should have a satisfactory frequency invariant property for the interested frequency band, which is dependent on the required shape $P(\sin\theta)$ of the beam and the temporal/spatial dimension of the corresponding 2-D filter. The more complicated the shape, the more coecients we need in each of the frequency invariant beams, i.e., a larger $M$ and $J$.

From the discussion of the last section, the desired beam response can be derived from the corresponding prototype filter $H(e^{j\Omega})$. Suppose the length of filter is $N$. As the shape is decided by the prototype filter, the dimension $M$ and $J$ of the 2-D fan filter (frequency invariant beamformer) should be at least 3 times that of the prototype filter to maintain the shape of the response of the prototype filter, that is, $N \le \min\{\frac{M}{3}, \frac{J}{3}\}$ [5].

Secondly, the beams formed should not be linearly dependent. Otherwise, some of the beam outputs will be a linear combination of the others, which leads to a waste of resources and also reduces the number of effective beams. As a result, we will not be able to null out the desired number of interfering signals. This second condition is not mentioned explicitly in [5], but it is a necessary condition to fully exploit the potential of the beamspace adaptive array. We will see later that the beam direction arrangement in [5] guarantees the linear independence of the beams.

These two conditions are not independent and there is a close relationship between them. In the following, we will show that the number of independent beams formed $N_{ind}$ cannot exceed the length $N$ of the prototype FIR filter. We prove this by contradiction.

Suppose we can have $P > N$ independent beams formed by some prototype filters with a length $N$. These beams have a response of $H_p(e^{j\pi\sin\theta})$, $p = 0, 1, \ldots, P-1$. Each of them is derived from the corresponding prototype filter $H_p(e^{j\Omega})$, $p = 0, 1, \ldots, P-1$, with an impulse response of $\mathbf{h}_p = [h_{p,0}, h_{p,1}, \ldots, h_{p,N-1}]^T$, $p = 0, 1, \ldots, P-1$. These prototype filters $H_p(e^{j\Omega})$, $p = 0, 1, \ldots, P-1$ can further be derived from the same lowpass filter as discussed in the last section, or they can simply be some different filters.

Now consider the linear combination of the following form

$$\mathbf{0} = \alpha_0\mathbf{h}_0 + \alpha_1\mathbf{h}_1 + \cdots + \alpha_{P-1}\mathbf{h}_{P-1}, \tag{5}$$

where $\alpha_0, \cdots, \alpha_{P-1}$ are scalars to be found for this equation to hold. Taking the transpose of both sides and then multiplying the equation with the vector $[1\; e^{j\pi\sin\theta} \ldots e^{j(N-1)\pi\sin\theta}]^T$, we arrive at

$$0 = \alpha_0 H_0(e^{j\pi\sin\theta}) + \alpha_1 H_1(e^{j\pi\sin\theta}) + \cdots + \alpha_{P-1}H_{P-1}(e^{j\pi\sin\theta}), \tag{6}$$

where $H_p(e^{j\pi\sin\theta})$, $p = 0, 1, \ldots, P-1$ is exactly the response of those independent beams. Since they are independent, all the scalars $\alpha_0, \cdots, \alpha_{P-1}$ must be zero for (6) to hold, and then for (5) to hold, which means that $\mathbf{h}_p$, $p = 0, 1, \ldots, P-1$ are independent. However, as $P$ is larger than the length of each vector $\mathbf{h}_p$, the rank of the $N \times P$ matrix formed by $H = [H_0, H_1, \ldots, H_{P-1}]$ cannot be larger than $N$, that is, it is impossible for all of the vectors $\mathbf{h}_p$ to be independent. Thus, we reach a contradiction.

As the maximum rank of $\mathbf{H}$ is $N$, we can see from the proof that the maximum number of independent beams formed will be equal to the length $N$ of the prototype FIR filter. Clearly, although we can design as many frequency invariant beams as we want, only $N$ of them are independent and at most we can only null out $N-1$ interfering signals. As the array's interference cancellation ability is dependent on both the number of independent beams and the frequency invariant property, there is trade-off between these two factors for a fixed $M$ and $J$. We may choose a prototype filter with $N = \min\{\frac{M}{3}, \frac{J}{3}\}$ for a good frequency invariant property, but when the number of interferences increases and becomes larger than $(\min\{\frac{M}{3}, \frac{J}{3}\} - 1)$, the array will not be able to null out the additional interferences. Therefore we may need to sacrifice the frequency invariant property a little to increase $N$ and design more independent beams. The loss in frequency invariant property can be compensated by the gain in the increasing number of independent beams. As a result, the interference cancellation ability of the array is improved. We will give some results to show this trade-off in our simulations.

The next question is, provided the length of the prototype filter $N$, how to design $N$ independent frequency invariant beams. We will propose a DFT-modulated method in the next section with the beam directions uniformly distributed in the spatial space and their independence guaranteed inherently.

## 4. DFT-modulated Design of the Frequency Invariant Beamformers

Before we proceed further, we want to give a sufficient condition with which the $P$ beams formed by $P$ general prototype filters $\mathbf{h}_p$, $p = 0, 1, \ldots, P-1$ are linearly independent. This condition is stated as follows.

• **As long as for the $\hat{p}-th$ frequency response $H_{\hat{p}}(e^{j\Omega})$, $\hat{p} = 0, \ldots, P-1$, there exists a point $\Omega = \Omega_{\hat{p}}$, where $H_{\hat{p}}(e^{j\Omega_{\hat{p}}}) \neq 0$ and all the remaining frequency responses $H_{p\neq\hat{p}}(e^{j\Omega_{\hat{p}}}) = 0$, the set of frequency responses $H_p(e^{j\Omega})$, $p = 0, 1, \ldots, P-1$, and hence the set of beams formed by them will be linearly independent**.

The proof is given in the following. Consider the equation (5) again. Taking the transpose of both sides and then multiplying the equation with the vector $[1\, e^{j\Omega} \ldots e^{j(N-1)\Omega}]^T$, we arrive at

$$0 = \alpha_0 H_0(e^{j\Omega}) + \alpha_1 H_1(e^{j\Omega}) + \cdots + \alpha_{P-1} H_{P-1}(e^{j\Omega}), \tag{7}$$

For $\hat{p} = 0$, put the value $\Omega = \Omega_0$ into the above equation, we have

$$0 = \alpha_0 H_0(e^{j\Omega_0}) + \alpha_1 H_1(e^{j\Omega_0}) + \cdots + \alpha_{P-1} H_{P-1}(e^{j\Omega_0}) = \alpha_0 H_0(e^{j\Omega_0}) + 0 + \cdots + 0. \tag{8}$$

As $H_0(e^{j\Omega_0}) \neq 0$, we have $\alpha_0 = 0$. Similarly, we have $\alpha_p = 0$, $p = 0, 1, \ldots, P-1$. Therefore, for (7) to hold, all the $P$ scalars must be zero, that is, both the vectors $\mathbf{h}_p$ and frequency responses $H_p(e^{j\Omega})$ are linearly independent. The proof is complete.

In [5], the main direction of a beam was arranged to coincide with nulls (zero responses) of all other beams. From the above proof, clearly, this arrangement guarantees the independence of the beams. However, in [5], the authors were simply using the existing nulls of the prototype filter, so the direction of the auxiliary beams can not be controlled by the designer and they can point to anywhere depending on the chosen lowpass prototype filter. Here we propose a DFT-modulated method for the design of the independent frequency invariant beamformers, where the beam directions are uniformly distributed in the spatial domain and their independence is guaranteed inherently.

Assume the impulse response of a lowpass filter is $h[n]$, $n = 0, 1, \ldots, N-1$. Based on $h[n]$, we can obtain the response $\mathbf{h}_p$ of the $p-th$ prototype filter for the $p-th$ beam shape design by the following DFT modulation

$$h_{p,n} = h[n] e^{j\frac{2pn\pi}{P}}. \tag{9}$$

In the frequency domain, this modulation shifts the response of original prototype filter $h[n]$ along the frequency axis by $\frac{2p\pi}{P}$. If the $z$-transform $H(z)$ of $h[n]$ can be expressed as

$$H(z) = \prod_{p=1}^{P-1} (1 - e^{j\frac{2p\pi}{P}} z^{-1}), \tag{10}$$

then after modulation, the main direction of the $P$ resultant beams will coincide with the nulls of the other beams, hence these beams will be independent. Note in this case, we have $P = N$, i.e., the number of independent beams formed will be the length of the prototype filter.

For the main directions of these beams, we have

$$\pi \sin\theta = \begin{cases} \frac{2p\pi}{P} & \text{for } \frac{2p\pi}{P} < \pi \\ \frac{2p\pi}{P} - 2\pi & \text{for } \frac{2p\pi}{P} \geq \pi \end{cases} \Rightarrow \sin\theta = \begin{cases} \frac{2p}{P} & \text{for } \frac{2p}{P} < 1 \\ \frac{2p}{P} - 2 & \text{for } \frac{2p}{P} \geq 1 \end{cases}, \tag{11}$$

for $p = 0, 1, \ldots, P-1$. They are uniformly distributed in the $\sin\theta$ domain, where the first beam point to the direction $sin\theta = 0$ will be the main beam and the others will be the auxiliary beams. Fig. 3 gives an example of the desired beam shapes with $P = N = 5$, where it can be seen clearly that each of the five beam directions coincides with the nulls of the other beams. Once we obtain the $P$ desired beam responses $H_p(e^{j\pi\sin\theta})$, we can follow the procedures given in [8] to obtain the coefficients of the corresponding beamformers.

One point to note is, in general, the $H_p(e^{j\pi\sin\theta})$ obtained by DFT modulation is of complex value for different $\theta$ that is,

$$H_p(e^{j\pi\sin\theta}) = A_p(\theta)e^{jB_p(\theta)} \tag{12}$$

where $A_p(\theta)$ and $B_p(\theta)$ are some real functions. The change of both $A_p(\theta)$ and $B_p(\theta)$ with respect to different $\theta$ will lead to a more complicated $(\Omega_1, \Omega_2)$ pattern for the design, which will require more coefficients in the temporal domain and therefore larger dimension of the array. As $A_p(\theta)$ contains enough information about the shape of the beam response, we can ignore the phase part $B_p(\theta)$ and our results show that in this way we can significantly improve the frequency invariant property of the beams with the same array dimensions.

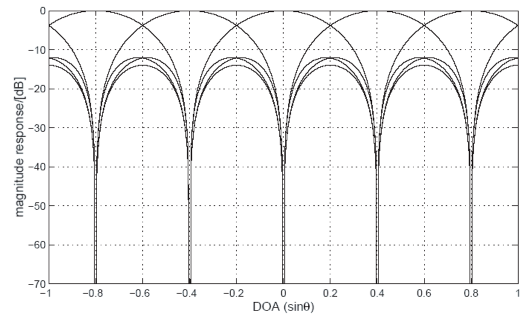


Figure 3: The desired beam shapes with $P = N = 5$ formed by DFT modulations.

## 5. Simulations

To show the trade-off between the frequency invariant property and the number of linear independent beams, the spatial and temporal dimensions of the frequency invariant beams are fixed as $M = 14$ and $J = 16$. According to [5], ideally we should use a prototype filter of length $\lfloor 14/3 \rfloor = 4$ for the design of the 4 FIBs. Fig. 4 shows the pattern of the main beam based on a 4-tap filter over the bandwidth $[0.4\pi; 0.9\pi]$.

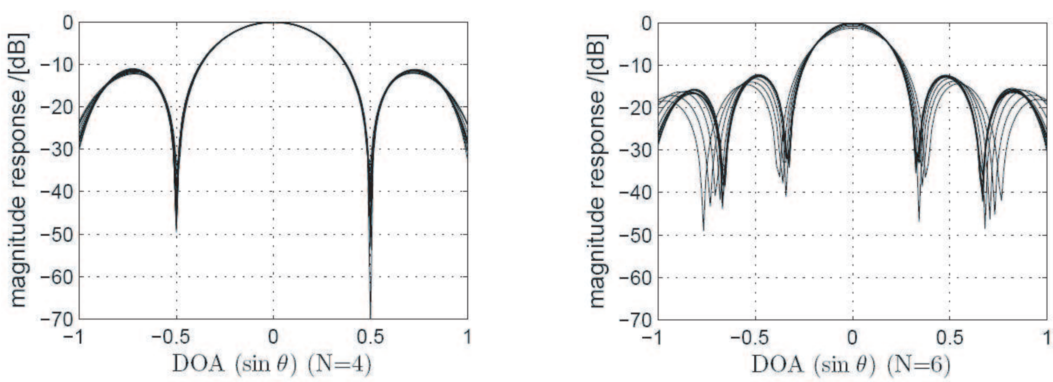


Figure 4: The magnitude response of the main beam over the bandwidth of $[0.4\pi; 0.9\pi]$, based on a 4-tap and a 6-tap prototype filter, respectively.

The signal of interest comes from broadside and with a signal to interference ratio (SIR) of -20 dB and signal to noise ratio (SNR) of 20 dB. Five interfering signals come from the angles of 20°, -25°, 45°, -50°, and -80°, respectively. Both the interfering signals and the signal of interest have a bandwidth of $[0.4\pi; 0.9\pi]$. We used a normalised LMS algorithm for adaptation. The learning curve with a stepsize of 0.01 is shown by the dashed line in Fig. 5. As the number of interfering signals are 5, which is larger than $4 - 1 = 3$, the number of auxiliary beams, the 4-beam adaptive array can not null out all of the interferences, although all of the beams have a very good frequency invariant response over the interested bandwidth $[0.4\pi; 0.9\pi]$. As a result, the learning curve only reaches a level of 15 dB. In order to improve its performance, we need to sacrifice the frequency invariant property a little. So, we increased the length $N$ of the prototype filter to 5, and 5 independent beams were obtained. The learning curve of this new system with the same stepsize is shown by the dotted line in Fig. 5. Compared to the 4-beam array, the ensemble mean square residual error has been reduced to about 8 dB. We can further to improve the performance of the system by designing 6 independent beams based on a 6-tap prototype filter ($N = 6$). The frequency invariant property of the main beam in this case is also shown in

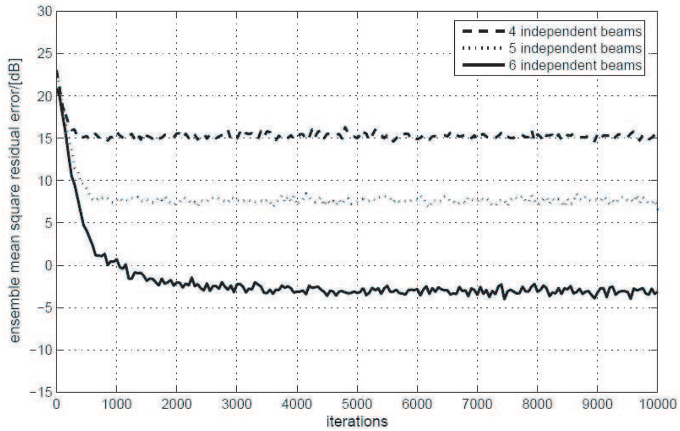


Figure 5: The learning curves for different number of independent beams.

Fig. 4, which is clearly not as good as that of $N = 4$. However, as there are more independent beams formed in this array, a further improvement of more than 10 dB has been achieved, as shown by the solid line in Fig. 5.

## 6. Conclusions

An analysis of the broadband beamspace adaptive array has been provided and it is shown that in order to improve the interference cancellation capability of the array, we may need to sacrifice the frequency invariant property of the beams to some degree for more linearly independent beams. We also proposed a DFT-modulated design of the frequency invariant beams employed in the broadband beamspace adaptive array, where the beam directions are uniformly distributed over the spatial domain and the linear independence of the beams is guaranteed inherently. Simulation results verified our analysis and the proposed method.

## Acknowledgement

This work was supported by the National Natural Science Foundation of China under grant 60325102 and 60428101.

**REFERENCES**

1. Godara, L. C., "Application of antenna arrays to mobile communications, Part II: Beam-forming and direction- of-arrival estimation," *Proceedings of the IEEE*, Vol. 85, No. 8, 1195–1245, August 1997.
2. Weiss, S., R. W. Stewart, M. Schabert, I. K. Proudler, and M. W. Hoffman, "An efficient scheme for broadband adaptive beamforming," *Proc. Asilomar Conference on Signals, Systems, and Computers*, Monterey, CA, Vol. I, 496–500, November 1999.
3. Neo, W. H. and B. Farhang-Boroujeny, "Robust microphone arrays using subband adaptive filters," *IEE Proceedings-Vision, Image and Signal Processing*, Vol. 149, No. 1, 17–25, February 2002.
4. Liu, W., S. Weiss, and L. Hanzo, "A subband-selective broadband gsc with cosine-modulated blocking matrix," *IEEE Transactions on Antennas and Propagation*, Vol. 52, 813–820, March 2004.
5. Sekiguchi, T. and Y. Karasawa, "Wideband beamspace adaptive array utilizing fir fan filters for multibeam forming," *IEEE Transactions on Signal Processing*, Vol. 48, No. 1, 277–284, January 2000.
6. Liu, W., S. Weiss, and L. Hanzo, "A generalised sidelobe canceller employing two-dimensional frequency invariant filters," *IEEE Trans. Antennas and Propagation*, Vol. 53, No. 7, 2339–2343, July 2005.
7. Takao, K. and K. Uchida, "Beamspace partially adaptive antenna," *IEE Proceddings H, Microwaves, Antennas and Propagation*, Vol. 136, 439–444, December 1989.
8. Liu, W. and S. Weiss, "A new class of broadband arrays with frequency invariant beam patterns," *Proc. IEEE International Conference on Acoustics, Speech, and Signal Processing*, Montreal, Canada, Vol. 2, 185–188, May 2004.

# A Subspace-based Robust Adaptive Capon Beamforming

**G. S. Liao**, **H. Q. Liu**, **and J. Li**
Xidian University, China

**Abstract**—Adaptive beamforming suffers from performance degradation in the presence of mismatch between the actual and presumed array steering vector of the desired signal. This idea enlightens us, so we propose a subspace approach to adaptive beamforming that is robust to array errors based on minimizing MUSIC output power. The proposed method involves two steps, the first step is to estimate the actual steering vector of the desired signal based on subspace technique, and the second is to obtain optimal weight by utilizing the estimated steering vector. Our method belongs to the class of diagonal loading, but the optimal amount of diagonal loading level can be calculated precisely based on the uncertainty set of the steering vector. To obtain noise subspace needs eigen-decomposition that has a heavy computation load and knows the number of signals *a priori*. In order to overcome this drawback we utilized the POR (Power of R) technique that can obtain noise subspace without eigen-decomposition and the number of signals *a priori*. It is very interesting that *Li Jian's* method is a special case where $m = 1$, and the proposed subspace approach is the case where $m \to \infty$, so we obtained a uniform framework based on POR technique. This is also an explanation why the performance of the proposed subspace approach excels that of *Li Jian's* method. The excellent performance of our algorithm has been demonstrated via a number of computer simulations.

## 1. Introduction

Array signal processing has wide applications in radar, communications, sonar, acoustics, seismology, and medicine. One of the important tasks of array processing is beamforming. The standard beamformers include the delay-and-sum approach, which is known to suffer from poor resolution and high sidelobe problems. The Capon beamformer adaptively selects the weight vectors to minimize the array output power subject to the linear constraint that the signal of interest (SOI) does not suffer from any distortion [1]. The Capon beamformer has better resolution and interference rejection capability than the standard beamformer, provided that the array steering vector corresponding to the SOI is accurately known. In practice, the knowledge of the SOI steering vector may be imprecise, the case due to differences between the presumed signal steering vector and the actual signal steering vector. When this happens, the Capon beamforming may suppress the SOI as an interference, which result in array performance drastically reduced, especially array output signal-to-interference-plus-noise ratio (SINR) [4].

In the past three decades many approaches have been proposed to improve the robustness of the Capon beamforming. Additional linear constraints, including point and derivative constraints, have been imposed to improve the robustness of the Capon beamforming [2, 3]. However, for every additional linear constraints imposed, the beamformer loses one degree of freedom (DOF) for interference suppression. Moreover, these constraints are not explicitly related to the uncertainty of the array steering vector. Diagonal loading (including its extended versions) has been a popular approach to improve the robustness of the Capon beamformer [4]. However, for most of the diagonal loading methods, determining the diagonal loading remains an open problem. Recently there are some methods been proposed (for examples, [5–7] and reference therein) to this point.

Mismatch between the presumed steering vector of the SOI and the actual one result in drastically reduced array SINR, therefore if we can estimate actual steering vector of the SOI, robustness of the array will be improved. In this paper, from the point of view of the subspace we propose a novel robust Capon beamformer, which involves two steps, the first step is to estimate actual steering vector of SOI, and the second is to calculate optimal weight by Capon method. The rest of this paper is organized as follows. Section 2 contains background material. In section 3, the robust Capon beamformer is developed. Computer simulation results illustrating the performance of the robust Capon beamformer are presented in Section 4. Finally, Section 5 contains the conclusions.

## 2. Background

### 2.1. Signal Model

We consider the standard narrowband beamforming model in which a set of $M$ narrowband plane wave signals, impinge on an array of $N$ sensors with half wavelength spacing, where $M < N$. The $N \times 1$ vector of received signals is given by

$$\mathbf{x}(t_k) = \sum_{m=0}^{M-1} \mathbf{a}(\theta_m) s_m(t_k) + \mathbf{n}(t_k), \quad k = 1, 2, \ldots, L \tag{1}$$

where $s_m(t_k), m = 0, \ldots, M-1$; $k = 1, 2, \ldots, L$ are the source signals snapshots,

$$\mathbf{a}(\theta_m) = [1, e^{-j\pi \sin\theta_m}, \ldots, e^{-j\pi(N-1)\sin\theta_m}]^T$$

is the steering vector in the direction $\theta_m$, and $\mathbf{n}(t_k)$, $k = 1, 2, \ldots, L$ are the vectors containing additive white noise samples, $L$ is the number of the snapshots. Also, in this paper, the sources and noise are assumed to be statistically uncorrelated.

We assume that one of the signals is the desired signal, say $s_0(t)$, and treat the remaining signals as interferences. Since $s_0(t)$ is uncorrelated with the noise and interferences, the data covariance matrix has the form,

$$\mathbf{R} = \sigma_0^2 \mathbf{a}(\theta_0)\mathbf{a}^H(\theta_0) + \sum_{k=1}^{M-1} \sigma_k^2 \mathbf{a}(\theta_k)\mathbf{a}^H(\theta_k) + \mathbf{R}_n \triangleq \mathbf{R}_s + \mathbf{R}_{i+n} \tag{2}$$

where $\mathbf{R}_s = \sigma_0^2 \mathbf{a}(\theta_0)\mathbf{a}^H(\theta_0)$, $\sigma_i^2 = E\{|s_i(t_k)|^2\}$ is the power of $i$th signal, and $\mathbf{R}_{i+n}$ is the interference plus noise covariance matrix. In practice, the covariance matrix $\mathbf{R}$ is estimated by

$$\hat{\mathbf{R}} = \frac{1}{L} \sum_{n=1}^{L} \mathbf{x}_n \mathbf{x}_n^H \tag{3}$$

where all received signals have zero means and $L$ samples are independent.

### 2.2. Capon Beamforming

The Capon beamforming is as follows.

Determine the $N \times 1$ vector $\mathbf{w}_0$ that is the solution to the following linearly constrained quadratic minimization problem,

$$\min_{\mathbf{w}} \mathbf{w}^H \mathbf{R} \mathbf{w} \quad s.t. \mathbf{w}^H \bar{\mathbf{a}}(\theta_0) = 1 \tag{4}$$

where $\bar{\mathbf{a}}(\theta_0)$ is presumed steering vector of the desired signal.

Appling Lagrange multiplier method results in the following solution,

$$\mathbf{w}_0 = \frac{\mathbf{R}^{-1}\bar{\mathbf{a}}(\theta_0)}{\bar{\mathbf{a}}^H(\theta_0)\mathbf{R}^{-1}\bar{\mathbf{a}}(\theta_0)} \tag{5}$$

The array mean output power $p_0$ is

$$p_0 = \frac{1}{\bar{\mathbf{a}}^H(\theta_0)\mathbf{R}^{-1}\bar{\mathbf{a}}(\theta_0)} \tag{6}$$

The Capon beamformer has better resolution and much better interference rejection capability than the standard beamformer, provided that the presumed array steering vector of the SOI match actual array steering vector precisely. In practice, the exact steering vector of the SOI is unavailable or its measure/estimation is imprecise, therefore, we only use the presumed $\bar{\mathbf{a}}(\theta_0)$ instead of the actual $\mathbf{a}(\theta_0)$ in the Capon beamformer, and the mismatch between the exact steering vector and the presumed one may drastically degrade the performance of the Capon beamformer.

The array output SINR can be written as,

$$SINR = \frac{E[|\mathbf{w}_0^H \mathbf{s}_0(t)|^2]}{\mathbf{w}_0^H \mathbf{R}_{i+n} \mathbf{w}_0} = \frac{\sigma_0^2 |\mathbf{w}_0^H \mathbf{a}(\theta_0)|^2}{\mathbf{w}_0^H \left( \sum\limits_{k=1}^{M-1} \sigma_k^2 \mathbf{a}(\theta_k)\mathbf{a}^H(\theta_k) + \mathbf{R}_n \right) \mathbf{w}_0} \tag{7}$$

where $\sigma_0^2 = E(|s_0(t)|)$. Inserting (5) into (7) yields,

$$SINR = \sigma_0^2 \frac{\left|\bar{\mathbf{a}}^H(\theta_0)\mathbf{R}_{i+n}^{-1}\mathbf{a}(\theta_0)\right|^2}{\bar{\mathbf{a}}^H(\theta_0)\mathbf{R}_{i+n}^{-1}\bar{\mathbf{a}}(\theta_0)} \tag{8}$$

where $\mathbf{a}(\theta_0)$ is the actual steering vector, then (8) can be rewritten as:

$$\begin{aligned} SINR &= \sigma_0^2 \mathbf{a}^H(\theta_0)\mathbf{R}_{i+n}^{-1}\mathbf{a}(\theta_0) \times \frac{\left|\mathbf{a}^H(\theta_0)\mathbf{R}_{i+n}^{-1}\bar{\mathbf{a}}(\theta_0)\right|^2}{(\mathbf{a}^H(\theta_0)\mathbf{R}_{i+n}^{-1}\mathbf{a}(\theta_0))(\bar{\mathbf{a}}^H(\theta_0)\mathbf{R}_{i+n}^{-1}\bar{\mathbf{a}}(\theta_0))} \\ &= SINR_m \cdot \cos^2(\mathbf{a}(\theta_0), \bar{\mathbf{a}}(\theta_0); \mathbf{R}_{i+n}^{-1}) \end{aligned} \tag{9}$$

where $SINR_m = \sigma_0^2 \mathbf{a}^H(\theta_0)\mathbf{R}_{i+n}^{-1}\mathbf{a}(\theta_0)$ and $\cos^2(\cdot)$ is defined as,

$$\cos^2(\mathbf{a}, \mathbf{b}; \mathbf{Z}) = \frac{\left|\mathbf{a}^H \mathbf{Z} \mathbf{b}\right|^2}{(\mathbf{a}^H \mathbf{Z} \mathbf{a})(\mathbf{b}^H \mathbf{Z} \mathbf{b})} \tag{10}$$

Clearly, $0 \leq \cos^2(\mathbf{a}, \mathbf{b}; \mathbf{Z}) \leq 1$. Therefore, array output SINR is reduced due to mismatch between the presumed steering vector of the SOI and its true value.

In recent years, diagonal loading (DL) is a popular approach to improving the robustness of Capon beamformer to the mismatch above. In DL methods, the data covariance $\hat{\mathbf{R}}$ is replaced by $\hat{\mathbf{R}} + \gamma \mathbf{I}$, where $\gamma$ is positive constant (see reference [4–6] for details). The DL method proposed in [4] is used in Section 4 for comparisons. In the following section, a novel robust beamforming is developed to alleviate the effects of the steering vector mismatch on the SINR performance of Capon beamformer.

## 3. Robust Capon Beamforming

The *robust beamforming problem* we will deal with in this paper can be briefly stated as follows: Extend the Capon beamformer so as to improve array output SINR even only an imprecise knowledge of steering vector $\mathbf{a}(\theta_0)$ is available. To simplify the notation, in what follows, we sometimes omit the argument $\theta$ of $\mathbf{a}(\theta)$ and $\bar{\mathbf{a}}(\theta)$. We assume that the only knowledge we have about $\mathbf{a}(\theta_0)$ is that it belongs to the following uncertainty [5]

$$[\mathbf{a}(\theta_0) - \bar{\mathbf{a}}]^H \mathbf{C}^{-1} [\mathbf{a}(\theta_0) - \bar{\mathbf{a}}] \leq 1 \tag{11}$$

where $\mathbf{C}$ are given positive definite matrix.

As shown above, array performance loses will occur in the presence of mismatch between the presumed and actual steering vectors of the SOI. If we estimate the actual steering vector of the SOI as more precise as we can, then performance of the beamformer will be improved. The proposed robust Capon beamforming is based on this idea. From subspace theory we know that the actual steering vector of desired signal is orthogonal to noise subspace, our approach is based on the optimizing the projection of signal steering vector onto noise subspace. The steering vector is normed as $||\mathbf{a}||^2 = \mathbf{a}^H \mathbf{a} = N$. To derive our robust Capon beamformer, we use following constrained optimization

$$\begin{aligned} &\min_{\mathbf{a}} \mathbf{a}^H \mathbf{U}_n \mathbf{U}_n^H \mathbf{a} \\ &s.t.(\mathbf{a} - \bar{\mathbf{a}})^H C^{-1} (\mathbf{a} - \bar{\mathbf{a}}) \leq 1 \\ &||\mathbf{a}||^2 = N \end{aligned} \tag{12}$$

where $\bar{\mathbf{a}}$ is known to us in advance, but has error (mismatch to the actual steering vector of the SOI). $\mathbf{U}_n$ is the noise subspace, which is obtained by the eigen-decomposition of $\hat{\mathbf{R}}$. To make up the noise subspace, we assume that the number $M$, of plane waves impinging on the array is known *a priori*. We use this assumption only for derivations and cancel it later. Note that we can improve the estimation accuracy of the actual steering vector of the SOI from (12), and then obtain optimal weight $\mathbf{w}_0$ by Capon method.

Without loss of generality, we will consider solving (12) for the case in which $\mathbf{C} = \varepsilon \mathbf{I}$, ($\varepsilon$ is user parameter), then, (12) becomes

$$\begin{aligned} &\min_{\mathbf{a}} \mathbf{a}^H \mathbf{U}_n \mathbf{U}_n^H \mathbf{a} \\ &s.t.||\mathbf{a} - \bar{\mathbf{a}}||^2 \leq \varepsilon \\ &||\mathbf{a}||^2 = N \end{aligned} \tag{13}$$

We use the *Lagrange multiplier methodology* again, which is based on the function

$$L(\mathbf{a}, \lambda, \mu) = \mathbf{a}^H \mathbf{U}_n \mathbf{U}_n^H \mathbf{a} + \mu(2N - \varepsilon - \bar{\mathbf{a}}^H \mathbf{a} - \mathbf{a}^H \bar{\mathbf{a}}) + \lambda(\mathbf{a}^H \mathbf{a} - N) \tag{14}$$

where $\mu \geq 0$, $\lambda \geq 0$ are the *Lagrange multiplier*.

Hence, the unconstrained minimization of (14) for fixed $\mu$, $\lambda$, is given by

$$\frac{\delta L(\mathbf{a}, \mu, \lambda)}{\delta \mathbf{a}} = 2\mathbf{U}_n \mathbf{U}_n^H \mathbf{a} - 2\mu \bar{\mathbf{a}} + 2\lambda \mathbf{a} = 0 \tag{15}$$

Clearly, the optimal solution of $\mathbf{a}$ is

$$\hat{\mathbf{a}} = \mu(\mathbf{U}_n \mathbf{U}_n^H + \lambda \mathbf{I})^{-1} \bar{\mathbf{a}} \tag{16}$$

Inserting $\hat{\mathbf{a}}$ into (14), minimizing $L(\mathbf{a}, \lambda, \mu)$ with respect to $\mu$ gives

$$\frac{\delta L(\hat{\mathbf{a}}, \mu, \lambda)}{\delta \mu} = 2N - \varepsilon - \bar{\mathbf{a}}^H \hat{\mathbf{a}} - \hat{\mathbf{a}}^H \bar{\mathbf{a}} = 0 \tag{17}$$

Then, we obtain

$$\hat{\mu} = \frac{2N - \varepsilon}{2\bar{\mathbf{a}}^H (\mathbf{U}_n \mathbf{U}_n^H + \lambda \mathbf{I})^{-1} \bar{\mathbf{a}}} \tag{18}$$

Inserting $\hat{\mu}$ into (14), minimizing Lagrange function with respect to $\lambda$ yields

$$\frac{\delta L(\hat{\mathbf{a}}, \hat{\mu}, \lambda)}{\delta \lambda} = \hat{\mathbf{a}}^H \hat{\mathbf{a}} - N = 0 \tag{19}$$

and the following equation can be derived,

$$\frac{\bar{\mathbf{a}}^H (\mathbf{U}_n \mathbf{U}_n^H + \hat{\lambda} \mathbf{I})^{-2} \bar{\mathbf{a}}}{[\bar{\mathbf{a}}^H (\mathbf{U}_n \mathbf{U}_n^H + \hat{\lambda} \mathbf{I})^{-1} \bar{\mathbf{a}}]^2} = \frac{N}{(N - \frac{\varepsilon}{2})^2} \tag{20}$$

Then, the solution of $\hat{\lambda}$ can be obtained by some simple manipulations.

Substituting (18) into (16) yields

$$\hat{\mathbf{a}} = (N - \frac{\varepsilon}{2}) \frac{(\mathbf{U}_n \mathbf{U}_n^H + \hat{\lambda} \mathbf{I})^{-1} \bar{\mathbf{a}}}{\bar{\mathbf{a}}^H (\mathbf{U}_n \mathbf{U}_n^H + \hat{\lambda} \mathbf{I})^{-1} \bar{\mathbf{a}}} \tag{21}$$

To summarize, the proposed robust Capon beamforming consists of following steps.

**The algorithm**:

Step 1: Calculate data covariance matrix, i.e.,

$$\hat{\mathbf{R}} = \frac{1}{L} \sum_{n=1}^{L} \mathbf{x}_n \mathbf{x}_n^H$$

Step 2: Compute the eigen-decomposition of $\hat{\mathbf{R}}$ and obtain the noise subspace $\mathbf{U}_n$.

Step 3: Solve $\hat{\lambda}$ in (20).

Step 4: Use the $\hat{\lambda}$ in Step 3 to calculate

$$\hat{\mathbf{a}} = (N - \frac{\varepsilon}{2}) \frac{(\mathbf{U}_n \mathbf{U}_n^H + \hat{\lambda} \mathbf{I})^{-1} \bar{\mathbf{a}}}{\bar{\mathbf{a}}^H (\mathbf{U}_n \mathbf{U}_n^H + \hat{\lambda} \mathbf{I})^{-1} \bar{\mathbf{a}}} \tag{22}$$

Step 5: Compute optimal weight by Capon method, i.e.,

$$\mathbf{w}_0 = \alpha \hat{\mathbf{R}}^{-1} \hat{\mathbf{a}}, \quad \alpha = \frac{1}{\hat{\mathbf{a}}^H \hat{\mathbf{R}}^{-1} \hat{\mathbf{a}}} \tag{23}$$

The proposed robust beamforming belongs to the class of diagonal loading, but the optimal amount of diagonal loading level can be precisely calculated based on the uncertainty set of the steering vector. In the Section 4 computer simulation results demonstrate excellent performance of the proposed algorithm.

In order to avoid eigen-decomposition and knowing the number of signals *a priori*, we use the POR approach to obtain noise subspace. In [8], $\mathbf{R}$ is decomposed by EVD as

$$\mathbf{R} = [\mathbf{U}_s \ \mathbf{U}_n] \begin{bmatrix} \Lambda_s + \sigma_v^2 \mathbf{I} & \mathbf{0} \\ \mathbf{0} & \sigma_v^2 \mathbf{I} \end{bmatrix} \begin{bmatrix} \mathbf{U}_s^H \\ \mathbf{U}_n^H \end{bmatrix} \tag{24}$$

where $\Lambda_s = diag\{\delta_1^2, \ldots, \delta_M^2\}$, $\mathbf{U}_s$ denotes the signal subspace. It approximates the noise subspace of $\mathbf{R}$ based on $\mathbf{R}^{-m}$ ($m$ is a positive integer). Accordingly

$$\sigma_v^{2m} \mathbf{R}^{-m} = \mathbf{U}_n \mathbf{U}_n^H + \mathbf{U}_s diag\Big\{ \Big( \frac{\sigma_v^2}{\delta_i^2 + \sigma_v^2} \Big)^m \Big\} \mathbf{U}_s^H \tag{25}$$

Clearly, $(\sigma_v^2/(\delta_i^2+\sigma_v^2))^m$ is less than 1 and converge to zero for sufficiently large $m$. Theoretically, $\lim_{m\to\infty} \sigma_v^{2m} \mathbf{R}^{-m} = \mathbf{U}_n \mathbf{U}_n^H$. As result, we modify the criterion (12) and consider the following POR cost function

$$\begin{aligned} &\min_{\mathbf{a}} \mathbf{a}^H \hat{\mathbf{R}}^{-m} \mathbf{a} \\ &s.t. ||\mathbf{a} - \bar{\mathbf{a}}||^2 \le \varepsilon \\ &||\mathbf{a}||^2 = N \end{aligned} \tag{26}$$

By contrast, the (26) avoids estimating that dimension directly. Moreover, as $m \to \infty$, the proposed the POR beamforming method in (26) converges to the subspace one in (12), and it can be shown that the performance of the POR method for finite $m$ will converge to the subspace one through computer simulation. We compared our method with previous one in [6], where $m = 1$ in the section 4.

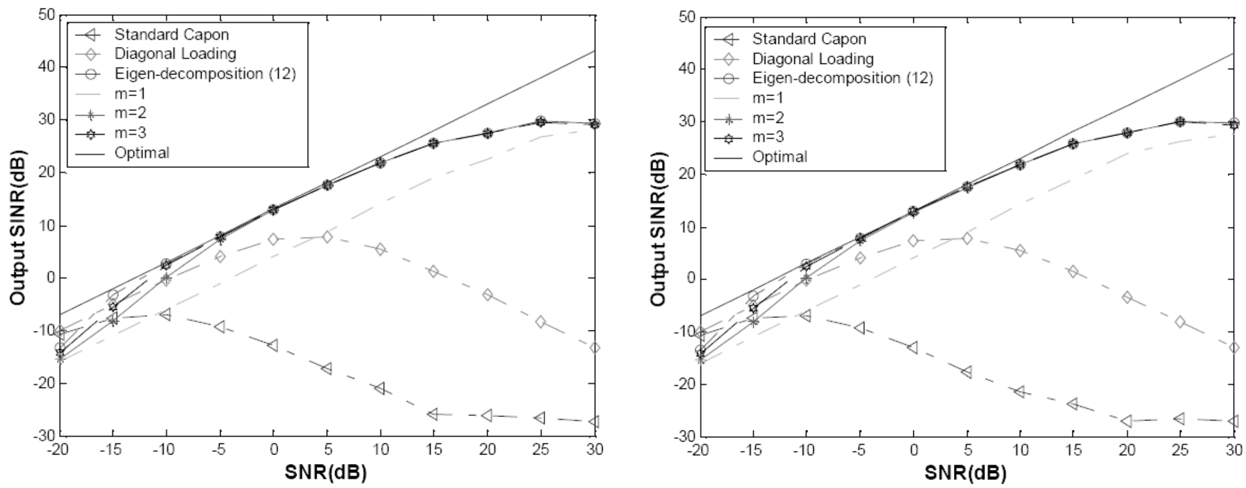


(a) (b)

Figure 1: Output SINR versus different SNR, pointing errors $\Delta = 3°$, for (a) $\varepsilon = 0.7$, for (b) $\varepsilon = 7$.

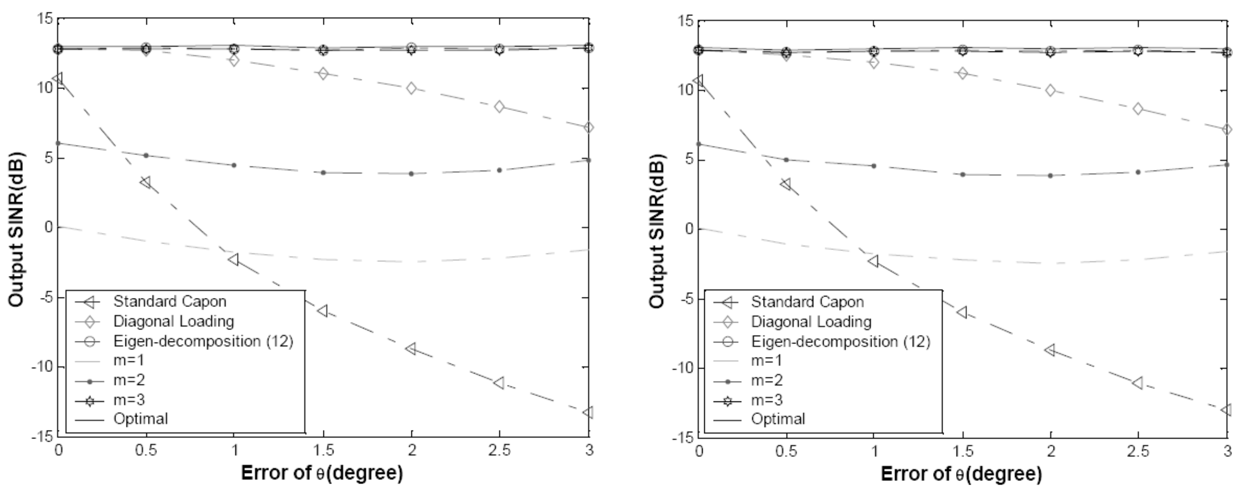


(a) (b)

Figure 2: The Output SINR versus pointing errors for (a) $\varepsilon = 0.7$, for (b) $\varepsilon = 7$.

## 4. Computer Results

Our main motivation of simulation is to demonstrate the performance in the presence of some errors in the steering vector. In all of the examples considered below, we assume a uniform linear array (ULA) with $N = 20$ sensors and half-wavelength spacing is used. The sources emitted mutual independent narrowband waveforms. All the results are achieved via 50 Monte Carlo trials.

In the first example, we consider the effect of the pointing error of the SOI on array output SINR. The exact direction of arrival of SOI is $\theta_0$, of which assumed value is $\theta_0 + \Delta$, i.e., $\bar{\mathbf{a}}(\theta_0) = \mathbf{a}(\theta_0 + \Delta)$. We assume that $\mathbf{a}(\theta_0)$ belongs to the uncertainty set

$$||\mathbf{a}(\theta_0) - \bar{\mathbf{a}}(\theta_0)||^2 \leq \varepsilon \tag{27}$$

where $\varepsilon$ is a user parameter. Let $\varepsilon_0 = ||\mathbf{a}(\theta_0) - \bar{\mathbf{a}}(\theta_0)||^2$. Then, choosing $\varepsilon = \varepsilon_0$. However, since $\Delta$ is unknown in practice, the $\varepsilon$ we choose may be greater or less than $\varepsilon_0$. To show that the choice of $\varepsilon$ is not a critical issue for our algorithm, we will present simulation results with several values of $\varepsilon$ in equation (21). In this example, the directions of the SOI and an interference source are $\theta_0 = 30°$, $\theta_1 = -30°$, respectively. The assumed direction of the SOI is $\theta_0 + \Delta = 33°$, which results exact $\varepsilon_0 = 5.7750$. The interference-to-noise ratio (INR) is 40 dB.

Figure 1 plots array output SINR versus the SNR of the SOI when the number of snapshots is set to be $L = 100$. It is observed that the proposed algorithm (12) performs better than other two algorithms at all input SNR. Also, since the error in steering vector of SOI is relatively large and cannot be negligible, the standard Capon beamformer and its diagonal loading version suffer from severe performance degradation when SNR increases. However, the proposed beamformer has SINR loss of 5 dB when SNR = 20 dB. The proposed the POR method for different $m$ over various input SNRs is also illustrated in Figure 1. Obviously, the Output SINR for $m = 2$ and $m = 3$ all converge to subspace approach (12), the counterpart for $m = 1$ [6] has the large output SINR loss.

Figure 2 shows the array output SINR curve versus the pointing errors, in which SNR = 0 dB, INR = 20 dB, $L = 100$. In this figure, the excellent performance achieved by the proposed algorithm is observed, which shows the robustness to the pointing errors. It is noted that, similar to other robust approaches, our method will worsen if there is/are strong interference spatially closed to the SOI. The reason is that for a given uncertainty region (11), the solution of $\mathbf{a}$ in optimization (12) is converge to the strong interference source. Also, it can be seen that the Output SINR of the proposed POR method increases as $m$ increases, with $m = 3$ has same performance with subspace one (12).

## 5. Conclusion

In this paper, we discuss the performance degradation due to the presence of steering vector uncertainty of the SOI, such as, direction of arrival estimation error, finite number of snapshots, and array response error, etc. A robust Capon beamformer is developed by utilizing the orthogonality between signal and noise subspace. A more accurate estimate of the actual steering vector of the SOI is obtained via constrained optimization, by which the optimal weight is computed according to Capon beamforming. We have shown that the proposed algorithm belongs to the class of diagonal loading approaches, and the optimal amounts of diagonal loading can be precisely calculated. In order to avoid eigen-decomposition and knowing the number of signals *a priori*, we have proposed a POR-based robust beamforming scheme. It significantly outperforms the method proposed in [6] and converge to the subspace one (12). The excellent performance of our algorithm has been demonstrated via a number of computer simulations.

## Acknowledgment

The work described in this paper was supported by National Science Fund under grant NFS60472097.

### REFERENCES

1. Capon, J., "High resolution frequency-wavenumber spectrum analysis," *Proc. IEEE*, Vol. 57, 1408–1418, Aug. 1969.
2. Er, M. H. and A. Cantoni, "Derivative constraints for broad-band element space antenna array processor," *IEEE Trans. Acoust., Speech, Signal Processing*, Vol. ASSP-31, 1378–1393, Dec. 1983.
3. Buckley, K. M. and L. J. Griffiths, "An adaptive generalized sidelobe canceller with derivative constraints," *IEEE Trans. Antennas Propagat.*, Vol. AP-34, 311–319, Mar. 1986.
4. Carlson, B. D., "Covariance matrix estimation errors and diagonal loading in adaptive arrays," *IEEE Trans. Aerospace and Electronic System.*, Vol. 24, 397–401, Jul. 1988.
5. Stoica, P., Z.-S. Wang, and J. Li, "Robust capon beamforming," *IEEE Signal Processing Letters*, Vol. 10, No. 6, 172–175, June 2003.
6. Li, J., P. Stoica, and Z.-S. Wang, "Doubly constrained robust capon beamforming," *IEEE Trans. Signal Processing*, Vol. 52, No. 9, 2407–2423, Sep. 2004.
7. Shahbazpanahi, S., A. B. Gershman, Z.-Q. Luo, and K. M. Wong, "Robust adaptive beamforming for general-rank signal models," *IEEE Trans. Signal Processing*, Vol. 51, No. 9, 2257–2269, Sep. 2003.
8. Xu, Z., P. Liu, and X. Wang, "Blind multiuser detection: from moe to subspace methods," *IEEE Trans. Signal Processing*, Vol. 52, No. 2, 510–524, Feb. 2004.

# Signal Processing of Pyroelectric Arrays for Industrial Laser Applications

**G. Biagini, L. Capineri, and L. Masotti**
Università di Firenze, Italy

**M. Mazzoni**
CNR-IFAC, Italy

Pyroelectric arrays are widely used for detection of UV-VIS and IR radiation. For their derivative sensor characteristic with respect to temperature their application is addressed to modulated and impulsive radiation. Also for this type of sensors, novel applications require detailed process study and custom signal processing.

For whichever industrial laser application, source diagnostic (temporal waveform, peak amplitude and beam pointing stability, divergence, power density mapping) is claimed, especially for the most involved parameters which determine the efficiency of the process.

Continuos Wave $CO_2$ laser systems used for cutting metal slabs have long tube arms of large section (5 cm diameter) with knobs supporting mirrors which necessitate to be aligned. To this aim the authors developed large area ($5 \times 5\,\mathrm{cm}^2$) $8 \times 8$ elements matrix arrays for a detailed evaluation of the laser spot inside the arm section and its centroid determination. As laser bursts of duration and delay depending on power are currently used for the alignment, we processed the sensor signal for the attainment of the temporal waveforms first of all. Due to the coherence of the laser source one array element is sufficient to diagnostic the laser temporal waveform for source diagnostic. Improved temporal resolution was obtained with special filters extending the flat response region of the sensor bandwidth to higher frequencies. We analysed the bursts and registered the time characteristic of CW regime attainment after the initial transient.

The signals from the matrix arrays were processed after this time by an ACF2101 Burr Brown (switched dual integrator) with *sample* & *hold* function synchronized for all array elements. The front-end analog electronics is formed by 64 dual integrators which, together with the sensors array, constitute the whole device that is fixed at the laser system arm sections. The integrated signals were A/D converted with 10 bits by an Hitachi 32 bit microcontroller equipped with 8 input ports switched by a multiplexer 1 to 8 in a separate device connected to the sensor head. In the electronic design, we optimised the degree of insulation in the hold phase, and we performed the evaluation of the off-set voltages and their influence both on the intensity distribution and the beam spot centroid determination. The first goal was reached by inserting a resistance in parallel with each element and an insulation better than 1% (corresponding to a current two order of magnitude lower than the maximum pyroelectric current).

The signal processing allows for matrix calibration trough normalisation of all the elements responses to the highest value measured in a preliminary calibration phase with a laser of high stability. Owing to the measured linearity in a wide power range (up to 1.5 kW) and different times integration (4–100) ms, the processing allows the choice of the proper time integration for better signal-to-noise ratios with different laser powers. The off-set voltages contributing with noise to an integrated signal also without laser bursts were suppressed by reciprocal subtraction of two-without and with laser burst- sequential acquisitions. Stability of centroid estimation of the order of 0.5 mm has been achieved with 1.5 kW CW Laser in industrial environment.

# Optimal Sensor Placement for the Localization of an Electrostatic Source

**B. A. Kemp, T. M. Grzegorczyk, and J. A. Kong**
Massachusetts Institute of Technology, USA

Electrostatic disturbance sensors have been developed for the passive detection and discrimination of charged bodies [1, 2]. Some proposed applications require the determination of source location or direction of arrival of a small charged object [2], which may be adequately modeled as a moving point charge. Source localization is an inverse problem in that the unknown coordinates of the electrostatic source at some instant in time are determined by the potential measurements from electrostatic disturbance sensors at known locations. This problem is solved by a multidimensional Newton search in the solution space. The solution is the iterative maximum likelihood (ML) estimator in additive white Gaussian noise (WGN), meaning that its performance is efficient in low noise. Since the estimator is iterative, a closed form expression for the solution variance cannot be determined. However, we show via numerical experiment that the iterative electrostatic localization estimator achieves the Cramer-Rao Lower Bound (CRLB) for low measurement noise. Therefore, the closed form expression of the CRLB can be used to represent the performance measure of the iterative estimator in low noise. We apply the expression for the CRLB to optimize the placement of electrostatic disturbance sensors such that for a specified estimator error tolerance, the sensor coverage is maximized at a known measurement noise level. We demonstrate the concept by numerical implementation for the 1D localization problem.

## REFERENCES

1. Zank, P. A., E. M. Sutphin, D. W. Buchanan, and T. G. Cehelnik, United States Patent No. 6,900,642, May 31, 2005.
2. Zank, P. A., E. M. Sutphin, D. W. Buchanan, and T. G. Cehelnik, United States Patent No. 6,922,059, July 26, 2005.

# Amplitude Estimation of Multichannel Signal in Spatially and Temporally Correlated Noise

**K. J. Sohn and H. Li**
Stevens Institute of Technology, USA
**B. Himed**
Air Force Research Laboratory/SNRT, USA

**Abstract**—This paper examines the problem of complex amplitude estimation of a multichannel signal in the presence of colored noise with unknown spatial and temporal correlation. A number of amplitude estimators are developed, including the optimum maximum likelihood (ML) estimator, which involves nonlinear optimization, and several suboptimal but computationally more efficient estimators based on least-squares (LS) or weighted LS (WLS) estimation. The Cramér-Rao bound (CRB) for the estimation problem is presented. Numerical results are presented to illustrate the performance of these estimators with or without training data.

## 1. Introduction

Amplitude estimation occurs in numerous signal processing applications. A survey of amplitude estimation techniques for sinusoidal signals with known frequencies in colored noise is found in [1]. While [1] is primarily concerned with *single-channel sinusoidal* signals, we consider amplitude estimation of an *arbitrary multichannel* signal observed in space and time using a sensor array. The observed data is contaminated by *a spatially and temporally correlated* disturbance signal with *unknown* correlation. Among other applications, this problem is encountered in an airborne radar system equipped with multiple antennas (e. g., [2]), where the multichannel signal refers to the space-time steering vector of the antenna array, the amplitude refers to the radar cross section (RCS) of a target, and the disturbance lumps together the thermal noise, radar clutter, and other interferences. Amplitude estimation within such a context would be useful for estimating the spatial and temporal correlation of the disturbance, developing effective target detectors, and finding solutions to several other relevant problems.

To account for its temporal and spatial correlation, our approach is to model the disturbance as a multichannel autoregressive (AR) process. Using extensive real radar data, [2] has shown that multichannel AR models are appropriate and offer efficient representation of the disturbance signal in airborne radars. Our *parametric* approach to the modeling of the disturbance is another major distinction compared to the *non-parametric* approach of [1]. Based on the parametric approach, our problem of interest is to find estimates of the signal amplitude, the AR coefficient matrices, and the spatial covariance matrix of the multichannel signal that drives the AR model. In the sequel, we first examine the optimum ML detector, and show that it involves nonlinear optimization. We then introduce several suboptimal but computationally more efficient LS and WLS amplitude estimators, which can be used to initialize the nonlinear searching involved in the ML estimator. The CRB for the estimation problem is presented as a performance baseline. In our numerical comparison of the different estimators, we focus on the case with *no or very limited training* data, which is of particular interest for applications in non-stationary or dense-target environments (e. g., [3]).

## 2. Data Model and Problem Statement

The observed noisy multichannel signal $\mathbf{x}_0(n)$ can be written as

$$\mathbf{x}_0(n) = \alpha\mathbf{s}(n) + \mathbf{d}(n), \quad n = 0, 1, \ldots, N-1, \tag{1}$$

where all vectors are $J\times 1$ vectors, $J$ is the number of spatial channels, $N$ is the number of temporal observations, $\mathbf{s}(n)$ denotes the signal vector that is assumed known but with unknown complex amplitude $\alpha$, and $\mathbf{d}(n)$ denotes the disturbance that is correlated in space and time. In addition, there are a set of *disturbance-only training* (i. e., $\alpha = 0$) data $\mathbf{x}_k(n)$, $k = 1, 2, \ldots, K$ and $n = 0, 1, \ldots, N-1$, available to assist amplitude estimation. In radar systems, training data may be obtained from range cells adjacent to the test cell. However, training is generally limited or may even be unavailable, especially in non-stationary or dense-target environments [3]. We consider amplitude estimation with and without training; in the later case, we have $K = 0$.

Let $\mathbf{x}_k \triangleq [\mathbf{x}_k^T(0), \mathbf{x}_k^T(1), \ldots, \mathbf{x}_k^T(N-1)]^T$, and $\mathbf{d}$ and $\mathbf{s}$ are formed similarly from $\mathbf{d}(n)$ and $\mathbf{s}(n)$, respectively. It is assumed that the training data $\{\mathbf{x}_k\}_{k=1}^K$ and $\mathbf{d}$ are independent and identically distributed (i.i.d.) with complex Gaussian distribution $\mathcal{CN}(\mathbf{0}, \mathbf{R})$, where $\mathbf{R}$ denotes the unknown space-time covariance matrix. A $J$-channel AR process is used to model the disturbance:

$$\mathbf{x}_k(n) - \alpha\mathbf{s}(n) = -\sum_{p=1}^{P} \mathbf{A}^H(p)\{\mathbf{x}_k(n-p) - \alpha\mathbf{s}(n-p)\} + \boldsymbol{\varepsilon}_k(n), \quad k = 0, 1, \ldots, K, \tag{2}$$

where $\{\mathbf{A}^H(p)\}_{p=1}^P$ denote the unknown $J \times J$ AR coefficient matrices and $\boldsymbol{\varepsilon}_k(n)$ denotes the driving spatial noise with distribution $\mathcal{CN}(\mathbf{0}, \mathbf{Q})$, where $\mathbf{Q}$ denotes the unknown $J \times J$ spatial covariance matrix. With some notational abuse, we have $\alpha = 0$ (i.e., disturbance-only) for $k \neq 0$ in (2). To focus on the amplitude estimation problem, we assume the model order $P$ is known. In practice when $P$ is unknown, it can be estimated by using a variety of model selection techniques [4].

The problem is to estimate the amplitude $\alpha$, which is the *signal parameter* of primary interest, as well as *nuisance parameters* $\{\mathbf{A}^H(n)\}$ and $\mathbf{Q}$, from observations $\{\mathbf{x}_k(n)\}$.

## 3. Amplitude Estimators

For compact presentation, let $\mathbf{A}^H \triangleq [\mathbf{A}^H(1), \ldots, \mathbf{A}^H(P)] \in \mathbb{C}^{J \times JP}$ which contains all the coefficient matrices involved in the $P$-th order AR model, $\mathbf{y}_k(n) \triangleq [\mathbf{x}_k^T(n-1), \ldots, \mathbf{x}_k^T(n-P)]^T$ which contains the regression subvectors formed from the observed signal $\mathbf{x}_0$ or the $k$-th training signal $\mathbf{x}_k$, and $\mathbf{t}(n) \triangleq [\mathbf{s}^T(n-1), \ldots, \mathbf{s}^T(n-P)]^T$, which contains the regression subvectors formed from the steering vector s. In the following, we first consider the optimal ML estimator, followed by the suboptimal LS and WLS estimators.

### 3.1. Optimal ML Amplitude Estimator

In Appendix 1, we show that the ML estimator of $\alpha$ is given by

$$\hat{\alpha}_{ML} = \min_{\alpha} \left| \hat{\mathbf{R}}_{xx}(\alpha) - \hat{\mathbf{R}}_{yx}^H(\alpha)\hat{\mathbf{R}}_{yy}^{-1}(\alpha)\hat{\mathbf{R}}_{yx}(\alpha) \right|, \tag{3}$$

where the correlation matrices are given by

$$\hat{\mathbf{R}}_{xx}(\alpha) = \sum_{n=P}^{N-1}[\mathbf{x}_0(n) - \alpha\mathbf{s}(n)][\mathbf{x}_0(n) - \alpha\mathbf{s}(n)]^H + \sum_{n=P}^{N-1}\sum_{k=1}^{K} \mathbf{x}_k(n)\mathbf{x}_k^H(n), \tag{4}$$

$$\hat{\mathbf{R}}_{yy}(\alpha) = \sum_{n=P}^{N-1}[\mathbf{y}_0(n) - \alpha\mathbf{t}(n)][\mathbf{y}_0(n) - \alpha\mathbf{t}(n)]^H + \sum_{n=P}^{N-1}\sum_{k=1}^{K} \mathbf{y}_k(n)\mathbf{y}_k^H(n), \tag{5}$$

$$\hat{\mathbf{R}}_{yx}(\alpha) = \sum_{n=P}^{N-1}[\mathbf{y}_0(n) - \alpha\mathbf{t}(n)][\mathbf{x}_0(n) - \alpha\mathbf{s}(n)]^H + \sum_{n=P}^{N-1}\sum_{k=1}^{K} \mathbf{y}_k(n)\mathbf{x}_k^H(n). \tag{6}$$

Although statistically optimal, there is no closed-form expression for the above ML estimate. The cost function (3) is a highly nonlinear bivariate function ($\alpha$ is complex-valued). A brute-force exhaustive search over the two-dimensional parameter space is generally impractical. Alternatively, we can resort to Newton-like iterative nonlinear searches, providing an initial estimate of $\alpha$ is available. Next, we discuss suboptimal estimators that can be used for initialization.

### 3.2. LS Estimator

A linear LS amplitude estimator based on $\mathbf{x}_0$ only is given by

$$\hat{\alpha}_{\mathrm{LS}} = \frac{\mathbf{s}^H\mathbf{x}_0}{\mathbf{s}^H\mathbf{s}}, \tag{7}$$

which ignores the coloredness of the disturbance signal. Albeit simple, the LS estimator is useful when training is unavailable. In addition, it can be used in combination with the WLS amplitude estimator presented next for improved estimation accuracy.

### 3.3. WLS Estimator

Suppose we have some initial estimates of $\mathbf{A}$ and $\mathbf{Q}$, denoted by $\hat{\mathbf{A}}$ and $\hat{\mathbf{Q}}$, respectively. Then, as shown in Appendix 2, a WLS amplitude estimator is given by

$$\hat{\alpha}_{\mathrm{WLS}} = \frac{\sum_{n=P}^{N-1}\{\mathbf{s}(n) + \sum_{p=1}^{P} \hat{\mathbf{A}}^H(p)\mathbf{s}(n-p)\}^H \hat{Q}^{-1}\{\mathbf{x}_0(n) + \sum_{p=1}^{P} \hat{A}^H(p)\mathbf{x}_0(n-p)\}}{\sum_{n=P}^{N-1}\{\mathbf{s}(n) + \sum_{p=1}^{P} \hat{\mathbf{A}}^H(p)\mathbf{s}(n-p)\}^H \hat{Q}^{-1}\{\mathbf{s}(n) + \sum_{p=1}^{P} \hat{A}^H(p)\mathbf{s}(n-p)\}}. \tag{8}$$

To find initial estimates $\hat{\mathbf{A}}$ and $\hat{\mathbf{Q}}$, we consider two cases with and without training. First, if training is available (i.e., $K \geq 1$), an ML estimator based on only the training data can be used to estimate $\mathbf{A}$ and $\mathbf{Q}$. Following similar steps in Appendix 1, we can show that the *training-only* ML *estimates* are given by

$$\hat{\mathbf{A}}^H = -\hat{\mathbf{R}}_{yx,t}^H \hat{\mathbf{R}}_{yy,t}^{-1}, \tag{9}$$

$$\hat{\mathbf{Q}} = \frac{1}{K(N-P)}\Big(\hat{\mathbf{R}}_{xx,t} - \hat{\mathbf{R}}_{yx,t}^H \hat{\mathbf{R}}_{yy,t}^{-1} \hat{\mathbf{R}}_{yx,t}\Big), \tag{10}$$

$\hat{\mathbf{R}}_{xx,t} = \sum_{n=P}^{N-1} \sum_{k=1}^{K} \mathbf{x}_k(n)\mathbf{x}_k^H(n)$, and $\hat{\mathbf{R}}_{yy,t}$ and $\hat{\mathbf{R}}_{yx,t}$ are correlation matrices formed similarly as in (5) and (6), however, using only the training signals.

On the other hand, if no training data are available ($K = 0$), we can create artificially one "training signal" by by subtracting. $\hat{\alpha}_{LS}\mathbf{s}(n)$ from the observed signal, i. e.,

$$\bar{\mathbf{x}}_0 \triangleq \mathbf{x}_0 - \hat{\alpha}_{LS}\mathbf{s}$$

where $\alpha_{LS}$ is given by (7). Then, the training-only ML estimator (9) and (10) can be used to estimate $\mathbf{A}$ and $\mathbf{Q}$ as if $K = 1$. Finally, it is noted that once the WLS estimate $\hat{\alpha}_{WLS}$ is obtained, it can be used to update estimates of $\mathbf{A}$ and $\mathbf{Q}$. We can iterate the above procedure a few times.

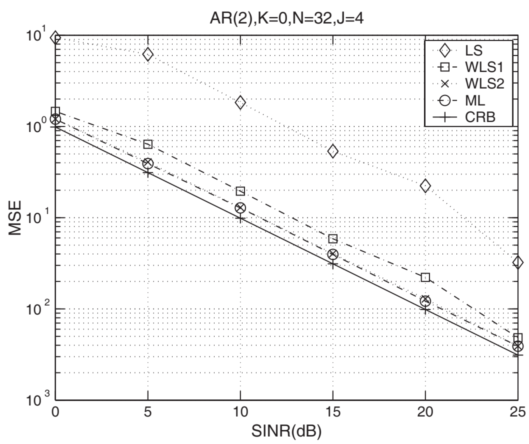


Figure 1: MSE of the signal amplitude estimate $\hat{\alpha}$ versus the input SINR when $J = 4$, $N = 32$, and $K = 0$.

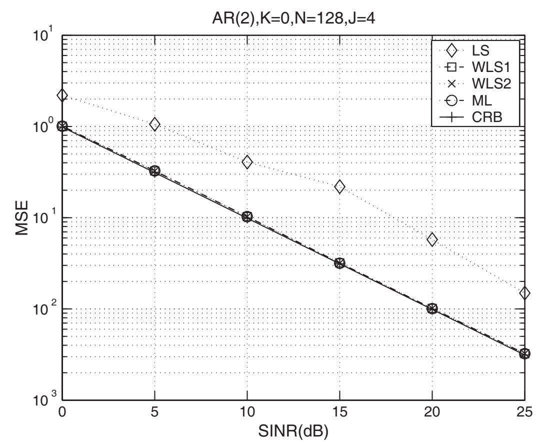


Figure 2: MSE of the signal amplitude estimate $\hat{\alpha}$ versus the input SINR when $J = 4$, $N = 128$, and $K = 0$.

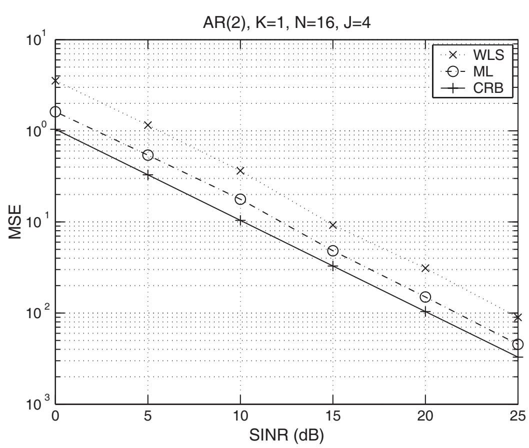


Figure 3: MSE of the signal amplitude estimate $\hat{\alpha}$ versus the input SINR when $J = 4$, $N = 16$, and $K = 1$.

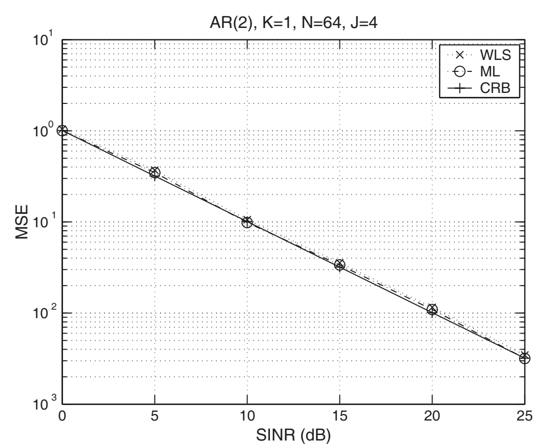


Figure 4: MSE of the signal amplitude estimate $\hat{\alpha}$ versus the input SINR when $J = 4$, $N = 64$, and $K = 1$.

## 4. Cramér-Rao Bound

The CRB provides a lower bound on the variance of the parameter estimates obtained by any unbiased estimators, and it can be used to access the accuracy of various amplitude estimation schemes. It can be shown that CRB for the signal amplitude estimation is given by

$$\mathrm{CRB}(\alpha) = \left[\sum_{n=P}^{N-1} \left\{\mathbf{s}(n) + \sum_{p=1}^{P} \mathbf{A}^H(p)\mathbf{s}(n-p)\right\}^H \mathbf{Q}^{-1} \left\{\mathbf{s}(n) + \sum_{p=1}^{P} \mathbf{A}^H(p)\mathbf{s}(n-p)\right\}\right]^{-1}. \tag{11}$$

## 5. Numerical Results

We present numerical results to compare the proposed amplitude estimation schemes. In the following, the SINR is defined as SINR= $|\alpha|^2\mathbf{s}^H\mathbf{R}^{-1}\mathbf{s}$ where $\mathbf{R}$ is the $JN \times JN$ joint space-time covariance matrix of the disturbance $\mathbf{d}$. For the no training case ($K = 0$), we consider 1) LS amplitude estimator given by (7); 2) WLS1 amplitude estimator given by (8) with estimates $\hat{\mathbf{A}}$ and $\hat{\mathbf{Q}}$ obtained by using the artificially created training signal; 3) WLS2 estimator which extends WLS1 with another iteration; 4) ML amplitude estimator given by (3). For the case when training is available ($K > 0$), we consider 1) WLS amplitude estimator given by (8) along with (9) and (10); 2) ML amplitude estimator given by (3). In both cases, the CRB (11) is included.

Figures 1 and 2 depict the mean-squared error (MSEs) of the various amplitude estimates versus the input SINR. We can see that 1) the MSE of WLS1 estimator is slightly larger than the CRB when $N = 32$, but is close to the CRB when $N = 128$; 2) as N increases, the MSEs of the WLS1, WLS2, and ML estimators are getting close to the CRB; 3) the MSE of the LS estimator is away from the CRB even at $N = 128$.

Figures 3 and 4 depict the MSEs of the various amplitude estimates versus the input SINR when very limited training is available ($K = 1$). It is seen that as $N$ increases, the WLS estimates are close to the ML estimates and the CRB.

## 6. Conclusion

We have examined the problem of amplitude estimation of a known multichannel signal in the presence of a temporally and spatially correlated disturbance signal. To deal with temporal and spatial coloredness, the disturbance signal is modeled as a multichannel AR process with unknown AR coefficient matrices and spatial covariance matrix. We have derived the ML estimate of the signal amplitude which involves two-dimensional nonlinear searches. We have also introduced several suboptimal LS and WLS estimators that can be utilized to initialize the searching.

### Appendix 1: Derivation of ML Estimators

The exact maximization of the joint PDF or likelihood function with respect to the unknown parameters produces a set of highly nonlinear equations that are difficult to solve. For large data records, the likelihood function can be well approximated by a joint conditional PDF (12) conditioned on $\{\mathbf{x}_k(n)\}_{n=0}^{P-1}\}, k = 0, 1, \ldots, K$ [5]. For brevity, the conditional PDF is referred to as the likelihood function henceforth. The loglikelihood function is proportional to (within an additive constant) [6]

$$\begin{aligned}
&-L\ln|\mathbf{Q}| - \sum_{k=1}^{K}\sum_{n=P}^{N-1}\left[\mathbf{x}_k(n) + \sum_{p=1}^{P}\mathbf{A}^H(p)\mathbf{x}_k(n-p)\right]^H \mathbf{Q}^{-1}\left[\mathbf{x}_k(n) + \sum_{p=1}^{P}\mathbf{A}^H(p)\mathbf{x}_k(n-p)\right] \\
&\quad - \sum_{n=P}^{N-1}\left[\{\mathbf{x}_0(n) - \alpha\mathbf{s}(n)\} + \sum_{p=1}^{P}\mathbf{A}^H(p)\{\mathbf{x}_0(n-p) - \alpha\mathbf{s}(n-p)\}\right]^H \mathbf{Q}^{-1} \\
&\quad \times\left[\{\mathbf{x}_0(n) - \alpha\mathbf{s}(n)\} + \sum_{p=1}^{P}\mathbf{A}^H(p)\{\mathbf{x}_0(n-p) - \alpha\mathbf{s}(n-p)\}\right]
\end{aligned} \tag{12}$$

where $L = (K+1)(N-P)$. Taking the derivative of the likelihood function with respect to $\mathbf{Q}$ and equating the result to zero produce the ML estimates of $\mathbf{Q}$ given $\alpha$ and $\mathbf{A}$:

$$\begin{aligned}
\hat{\mathbf{Q}}(\alpha, \mathbf{A}) \triangleq\ & \frac{1}{L}\left\{\sum_{k=1}^{K}\sum_{n=P}^{N-1}\left[\mathbf{x}_k(n) + \sum_{p=1}^{P}\mathbf{A}^H(p)\mathbf{x}_k(n-p)\right]\left[\mathbf{x}_k(n) + \sum_{p=1}^{P}\mathbf{A}^H(p)\mathbf{x}_k(n-p)\right]^H\right. \\
&+ \sum_{n=P}^{N-1}\left[\{\mathbf{x}_0(n) - \alpha\mathbf{s}(n)\} + \sum_{p=1}^{P}\mathbf{A}^H(p)\{\mathbf{x}_0(n-p) - \alpha\mathbf{s}(n-p)\}\right] \\
&\left.\times\left[\{\mathbf{x}_0(n) - \alpha\mathbf{s}(n)\} + \sum_{p=1}^{P}\mathbf{A}^H(p)\{\mathbf{x}_0(n-p) - \alpha\mathbf{s}(n-p)\}\right]^H\right\}.
\end{aligned} \tag{13}$$

Substituting the above $\hat{\mathbf{Q}}$ back in the likelihood function, we find that maximizing the loglikelihood reduces to minimizing $|\hat{\mathbf{Q}}(\alpha, \mathbf{A})|$. Therefore, the ML estimates of $\alpha$ and $\mathbf{A}$ can be obtained by minimizing $|\hat{\mathbf{Q}}(\alpha, \mathbf{A})|$ with respect to $\alpha$ and $\mathbf{A}$. In turn, we can get the ML estimate of $\mathbf{Q}$ by replacing $\alpha$ and $\mathbf{A}$ with their ML estimates in (13). Next, observe that

$$
\begin{aligned}
L\hat{\mathbf{Q}}(\alpha,\mathbf{A}) &= \hat{\mathbf{R}}_{xx}(\alpha)+\mathbf{A}^H\hat{\mathbf{R}}_{yx}(\alpha)+\hat{\mathbf{R}}_{yx}^H(\alpha)\mathbf{A}+\mathbf{A}^H\hat{\mathbf{R}}_{yy}(\alpha)\mathbf{A}\\
&= \left(\mathbf{A}^H+\hat{\mathbf{R}}_{yx}^H(\alpha)\hat{\mathbf{R}}_{yy}^{-1}(\alpha)\right)\hat{\mathbf{R}}_{yy}(\alpha)\left(\mathbf{A}^H+\hat{\mathbf{R}}_{yx}^H(\alpha)\hat{\mathbf{R}}_{yy}^{-1}(\alpha)\right)^H+\hat{\mathbf{R}}_{xx}(\alpha)-\hat{\mathbf{R}}_{yx}^H(\alpha)\hat{\mathbf{R}}_{yy}^{-1}(\alpha)\hat{\mathbf{R}}_{yx}(\alpha)
\end{aligned}
\tag{14}
$$

where the correlation matrices are given by (4), (5), and (6). Since $\hat{\mathbf{R}}_{yy}(\alpha)$ is non-negative definite and the remaining terms in (14) do not depend on $\mathbf{A}$, it follows that $\hat{\mathbf{Q}}(\alpha,\mathbf{A})\geq\hat{\mathbf{Q}}(\alpha,\mathbf{A})|_{\mathbf{A}=\hat{\mathbf{A}}(\alpha)}$, where

$$\hat{\mathbf{A}}^H(\alpha)=-\hat{\mathbf{R}}_{yx}^H(\alpha)\hat{\mathbf{R}}_{yy}^{-1}(\alpha). \tag{15}$$

When $\hat{\mathbf{Q}}(\alpha,\ \mathbf{A})$ is minimized, the estimate $\hat{\mathbf{A}}^H(\alpha)$ of $\mathbf{A}^H$ will minimize any non-decreasing function including the determinant of $\hat{\mathbf{Q}}(\alpha,\ \mathbf{A}))$ [7]. Hence, $\hat{\mathbf{A}}^H(\alpha)$ is the ML estimate of $\mathbf{A}^H$ given $\alpha$. Replacing $\mathbf{A}^H$ in (14) by $\hat{\mathbf{A}}^H(\alpha)$ yields the ML amplitude estimator (3).

**Appendix 2: Derivation of WLS Estimator**

Suppose that $\mathbf{Q}$ and $\mathbf{A}$ are known. Then, taking the derivative of the loglikelihood function (12) and setting the result to zero yield

$$
\begin{aligned}
&\alpha\sum_{n=P}^{N-1}\left\{\mathbf{s}(n)+\sum_{p=1}^{P}\mathbf{A}^H(p)\mathbf{s}(n-p)\right\}^H\mathbf{Q}^{-1}\left\{\mathbf{s}(n)+\sum_{p=1}^{P}\mathbf{A}^H(p)\mathbf{s}(n-p)\right\}\\
&-\sum_{n=P}^{N-1}\left\{\mathbf{s}(n)+\sum_{p=1}^{P}\mathbf{A}^H(p)\mathbf{s}(n-p)\right\}^H\mathbf{Q}^{-1}\left\{\mathbf{x}_0(n)+\sum_{p=1}^{P}\mathbf{A}^H(p)\mathbf{x}_0(n-p)\right\}=0.
\end{aligned}
\tag{16}
$$

By solving (16), we have the ML estimate of $\alpha$. It is different from the ML estimate (3) which assumes $\mathbf{Q}$ and $\mathbf{A}$ are unknown. In practice, $\mathbf{Q}$ and $\mathbf{A}$ are unknown. If these matrices are replaced by their estimates $\hat{\mathbf{Q}}$ and $\hat{\mathbf{A}}$, the resulting WLS estimator is given by (8).


## Acknowledgement

This work was supported by the Air Force Research Laboratory under contract number FA8750-05-2-0001.


### REFERENCES


1. Stoica, P., H. Li, and J. Li,, "Amplitude estimation of sinusoidal signals: survey, new results, and an application," *IEEE Transactions on Signal Processing*, Vol. 48, 338–352, February 2000.
2. Román, J. R., M. Rangaswamy, D. W. Davis, Q. Zhang, B. Himed, and J. H. Michels, "Parametric adaptive matched filter for airborne radar applications," *IEEE Transactions on Aerospace and Electronic Systems*, Vol. 36, No. 2, 677–692, April 2000.
3. Michels, J. H., B. Himed, and M. Rangaswamy, "Robust STAP detection in a dense signal airborne radar environment," *Signal Processing*, special issue on New Trends and Findings in Antenna Array Processing for Radar, Vol. 84, 1625–1636, 2004.
4. Söderström, T. and P. Stoica, *System Identification*, Prentice Hall International, London, UK, 1989.
5. Stoica, P., and R. L. Moses, *Spectral Analysis of Signals*, Upper Saddle River, Pearson Prentice Hall, NJ, 2005.
6. Sohn, K. J., H. Li, and B. Himed, "Parametric rao test for multichannel adaptive signal detection," submitted to *IEEE Transactions on Aerospace and Electronic Systems*, Prentice Hall International, London, UK, 2005.
7. Li, J., B. Halder, P. Stoica, and M. Viberg, "Computationally efficient angle estimation for signals with known waveforms," *IEEE Transactions on Signal Processing*, Vol. 43, No. 9, 2154–2163, September 1995.